RETENTION CHARACTERISTICS OF AUSTENITE IN AN INTER CRITICALLY ANNEALED LOW-CARBON, LOW ALLOY DUAL PHASE STEEL

by

Jyoti Prakash Chakravarty

A Thesis
presented to the University of Manitoba
in partial fulfillment of the
requirements for the degree of
Master of Science in Metallurgical Science
in
Department of Mechanical Engineering

Winnipeg, Manitoba, 1984

RETENTION CHARACTERISTICS OF AUSTENITE IN AN INTER CRITICALLY ANNEALED LOW-CARBON, LOW ALLOY DUAL PHASE STEEL

BY

JYOTI PRAKASH CHAKRAVARTY

A thesis submitted to the Faculty of Graduate Studies of the University of Manitoba in partial fulfillment of the requirements of the degree of

MASTER OF SCIENCE

ABSTRACT

Recent theoretical studies have shown that the presence of retained austenite in increasing amounts has a beneficial effect on the strength/ductility properties of intercritically annealed dual phase steels. These studies also indicated that improvement in the stability of this phase against deformation induced martensitic transformation also enhances these properties in such steels.

Investigations prior to these studies showed that the retention of this phase is due to the joint effects of chemical stabilization and austenite particle size effect. It was also observed experimentally that the stability of this phase against deformation induced transformation is primarily a function of its particle size. The stability increases with decreasing size.

In view of these findings, an experimental study was undertaken to determine the retention characteristics of austenite in such steels with the objective of optimizing the conditions under which increased amounts of retained austenite of superior stability can be retained. Variables in the form of annealing time, temperature and starting microstructure were considered in this study.

The results of this study indicate that the process of austenite formation is dominated by the nucleation kinetics up to 792°C temperature between A_1 temperature and 818°C. Beyond this temperature the austenite growth kinetics dominates the reaction process. This is true for samples with starting microstructure consisting of tempered martensite or ferrite + pearlite. However, in the case of samples with as quenched starting microstructure, this reaction is dominated only by

the nucleation kinetics of austenite in this annealing temperature range. For quenched and tempered starting microstructure it is found that up to a certain annealing time depending on the annealing temperature, the austenite formation is dominated by the nucleation kinetics beyond which the growth kinetics has an overriding effect.

It is also concluded from this study that a tempered martensitic starting microstructure yields significantly higher amounts of retained austenite of superior stability as compared to that obtained by using the conventional ferrite + pearlite starting microstructure. Furthermore it is seen that there exists a critical combination of annealing time and temperature corresponding to which maximum austenite is retained for samples with this starting microstructure.

ACKNOWLEDGEMENTS

I wish to express my sincere appreciation to Professor K. Tangri for guiding me with immense patience and constant encouragement throughout this work. My deep appreciation is also due to Dr. N.C. Goel, for all the pains he had undertaken to introduce me to the art of thesis writing and also for the helpful discussions we have had between us. The co-operation extended to me by Professor Ferguson and Mr. Neil Ball of the Earth Sciences Department of the University of Manitoba in carrying out some of the tests involved in this work is also appreciated. Thanks are also due to the Mechnical Engineering Department and Professor K. Tangri for the financial support given to me during this study. Finally, I would like to thank Messrs John Van Dorp, Don Mardis and Roy Hartle for their invaluable help.

TABLE OF CONTENTS

LIST OF FIGURES

CHAPTER I

INTRODUCTION AND OBJECTIVES

Dual Phase steels are a relatively new class of high strength low alloy (HSLA) steels developed in the mid 70's. They are characterized by a microstructure consisting of 15 to 25 vol % hard martensite (not pearlite as in conventional HSLA steels) dispersed as islands in a soft ferrite matrix. However, depending on the chemistry of the steel and the processing techniques employed, the second phase is often not martensite alone[1-3]. Instead, it may consist of a mixture of martensite, bainite and retained austenite (γ_R).

The production of these steels irrespective of the processing techniques used, consist of annealing low carbon-low alloy steels in the $\alpha + \gamma$ region (I.C. annealing) of the Fe-C equilibirum diagram followed by accelerated cooling.

These steels have superior ductility (Fig. 1) compared to conventional H.S.L.A. steels of equivalent strength[1-9]. They also exhibit a continuous yielding behaviour thus making them highly formable (Fig. 2). The effect of the dual phase microstructure on the ductility of these steels is an extremely complex subject because of the various factors that contribute to this property. Among them are, volume fraction of martensite[10-13,14], carbon content of martensite[12], plasticity of martensite, distribution of martensite[15], alloy content of ferrite[16,17-20], and retained austenite γ_R[21-26]. Of all these factors, attention in this study will be focussed on the contribution of γ_R since no significant attempt has been made to date to control ductility through the use of this phase.

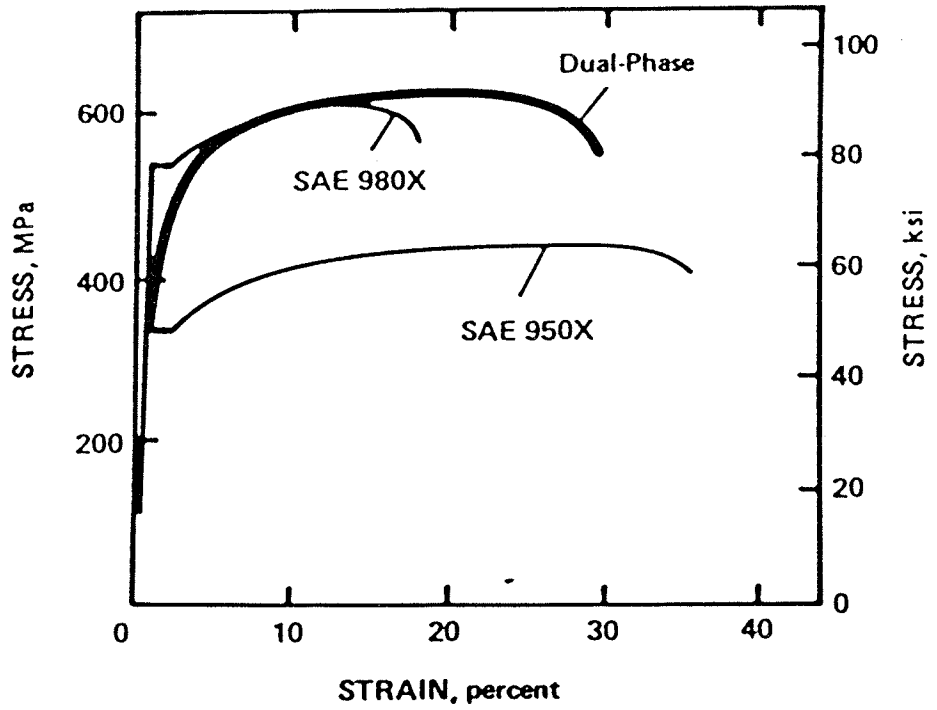

Figure 1. Stress-strain curves for HSLA and dual-phase steels[2]

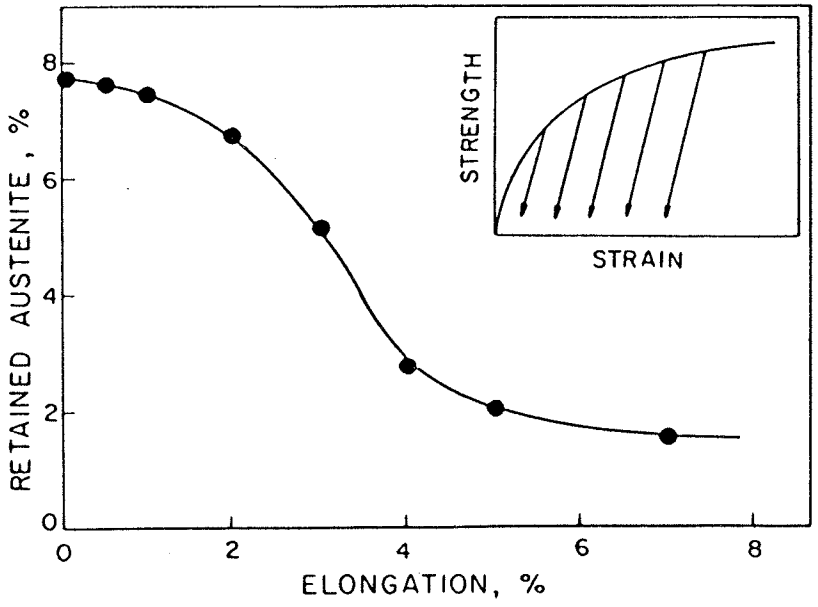

Figure 2. Retained Austenite as a function of strain for a Fe-0.07 C-1.8Mn-1.4Si Dual Phase Steel[35]

γ_R which may be present in amounts varying from 2 to 9 vol %[22,24,27,28], undergoes deformation induced martensitic transformation (DIMT), when these steels are deformed plastically (Fig. 2)[21,22,28,29]. When this phase is present in quantities of more than 4 vol %, it contributes to the improvement of the work hardening rates[29,30]. This phenomenon is similar to that observed in metastable austentic (TRIP) steels[31-34].

The correlation between γ_R and high work hardening rates, is based on the continuous transformation of retained austenite to martensite during deformation[21,22,35] and the dislocation structure generated by this transformation[3,5,36-38]. This aspect has been dealt with in detail[39-40], where it has been shown that the flow stress in steel is linearly proportional to the square root of the dislocation density. In the case of dual phase steels containing γ_R, the rate of increase of dislocation density per unit increase in strain exceeds that for a plain ferrite steel or ferrite + only martensite, containing dual phase steels at the same stain. Thus, the rate of work hardening ($d\sigma/d\varepsilon$) of these steels will exceed that for a plain ferrite or ferrite + martensite dual phase steel. A schematic representative of the situation is shown in figure 3[22]

That γ_R in dual phase steel is a very important microconstituent for producing high rates of work hardening is also evident from figure 4[22]. As per Considere's criterion, stable plastic flow will continue until the true stress (σ) exceeds the rate at which the matrix is able to work harden[41]. Thus the relationship:

$d\sigma/d\varepsilon > \sigma$ stable plastic flow

$d\sigma/d\varepsilon \leqq \sigma$ formation of neck

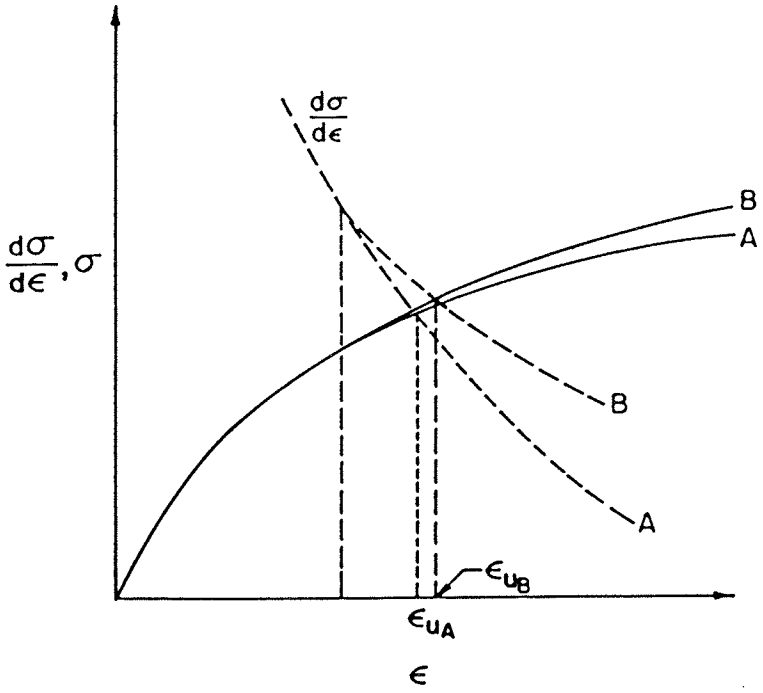

Figure 3. Schematic representation of the effect of strain induced transformation of γ_R to α' on the stress-strain curve of a D.P. Steel.

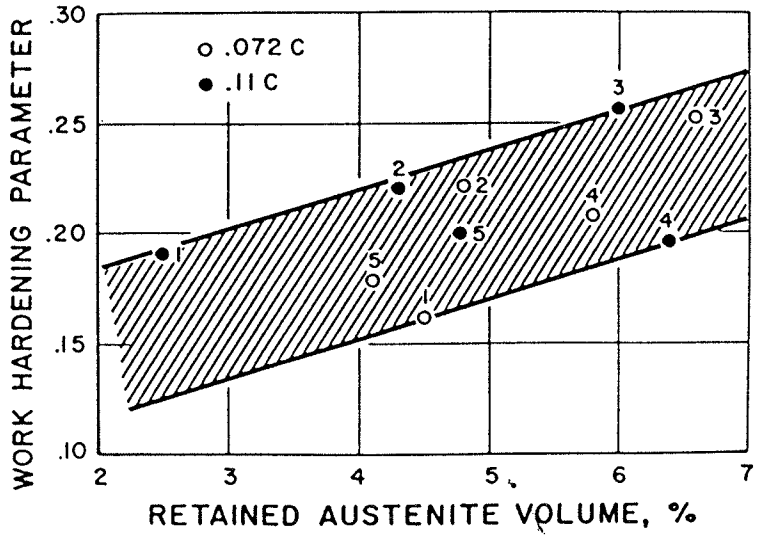

Figure 4. Variation in work hardening parameter with increasing retained austenite volume fraction[22]

The conditions are illustrated schematically in figure 3. The point of instability being $d\sigma/d\varepsilon = \sigma$, where necking sets in. The strain corresponding to this point is the maximum uniform elongation (εu). The establishment of high work hardening rates during the initial stages of straining increases the uniform elongation by delaying the onset of necking (Fig. 3). This is indicative of the fact that the stability of γ_R against DIMT is very intimately connected to the ductility of dual phase steels. It must be noted here, that for γ_R to make a positive contribution towards the ductility of these steels, it is essential that this phase has a moderate (neither very high nor very small) degree of stability against DIMT[42]. Insufficient stability will cause the flow stress to exceed the work hardening rate at low strains while in the case of extremely high stability, necking will set in before the martensite transformation process is initiated. Previous observations[21,22,28,35,43] hitherto show that this phase undergoes transformation during the early stages of plastic deformation characterizing poor stability against DIMT. Lately it has been observed that the 'ease' of this transformation is a function of the particle size of the γ_R phase[43]. As in the case of TRIP steels, the deformation induced transformation process becomes increasingly difficult as the austenite particle size becomes finer[44,45]. In addition to the moderate stability of γ_R, its increasing volume fraction has a cumulative effect in improving the strength and ductility of dual phase steels as has been shown in recent theoretical studies[42].

Although numerous studies in the past have established the presence of some amounts of retained austenite (which transforms to martensite during straining) in dual phase steels, no attempt to optimize the

volume fraction and stability of this phase have appeared in the literature. Therefore the aim of the present work was to make a systematic study and establish experimental conditions under which increasing amounts of austenite of improved stability can be retained.

CHAPTER II

LITERATURE REVIEW

The retention of austenite when steels are cooled from elevated temperatures has been attributed to the effects of one or more of the following stabilization mechanisms that may be operating. They are

a) Thermal Stabilization

b) Mechanical Stabilization

c) Chemical Stabilization

d) Stabilization due to austenite grain size effect

A thorough understanding of these mechanisms is necessary to be able to predict the conditions under which optimum amounts of austenite can be retained in dual phase steels. Therefore a critical review of these mechanisms is presented in the following subsection of this chapter.

2.1 Thermal Stabilization

Thermal stabilization of austenite is the inhibition of the martensite reaction resulting from an aging treatment. If during the normal thermal transformation from austenite to martensite the transformation is arrested and the partially transformed specimen is aged, thermal stabilization is manifested by the fact that upon subsequent cooling further transformation of martensite does not recommence at the arrest temperature (TA), but at a temperature below it. A proper measure of thermal stabilization is the magnitude of the temperature interval θ (Fig. 5) between the arrest temperature and the temperature at which athermal transformation recommences.

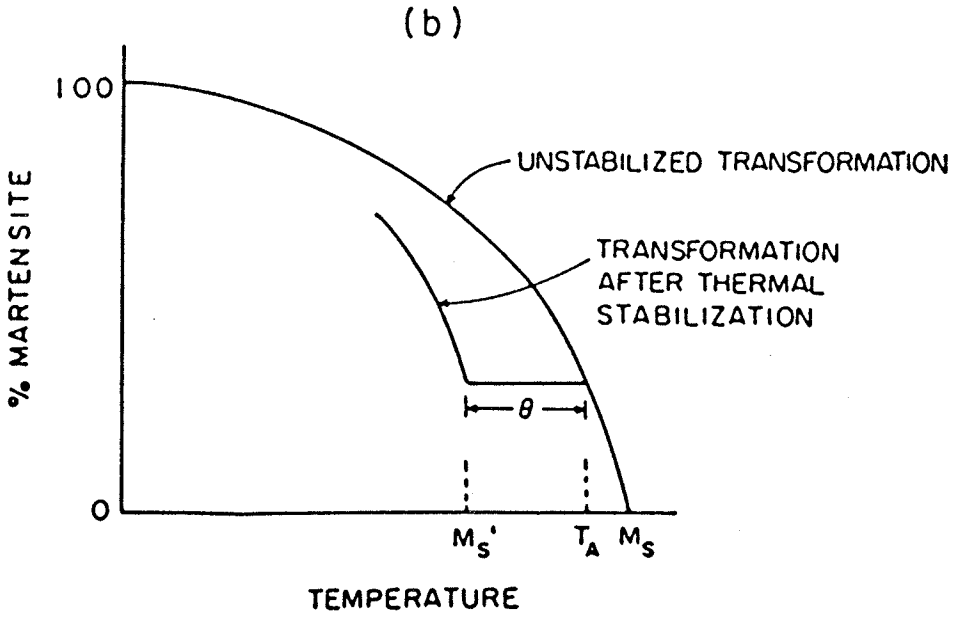

Figure 5. Effect of thermal stabilization as the progress of austenite-martensite transformation[65].

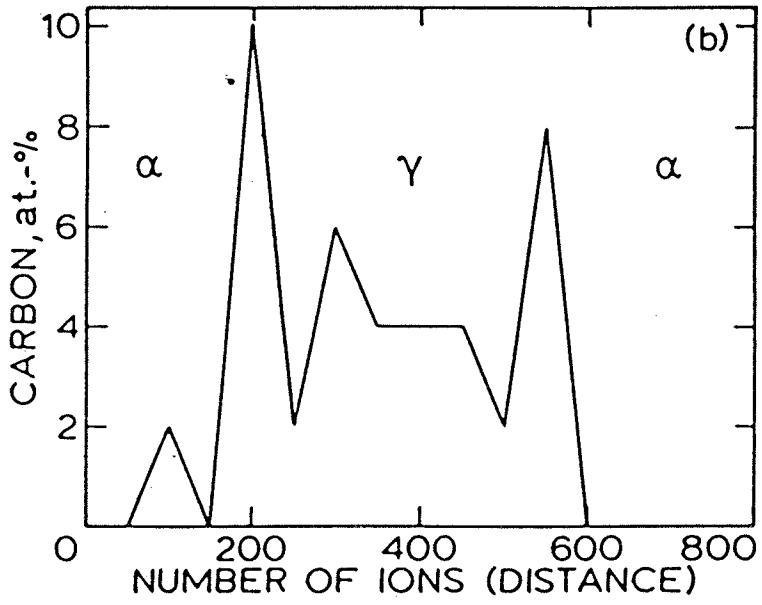

Figure 6. Distribution of carbon across the martensite/retained γ inter- face in a rapidly quenched 0.35%C steel[61].

It has been demonstrated that the extent of stabilization θ, of partially transformed specimens depends on the time and temperature of aging after the arrest[46,47,48]. The magnitude of θ as a function of time has been found to increase to a maximum value and then decrease at longer aging times in a manner analogous to overaging during solid state precipitation[48,49]. The most important feature of this phenomenon is that the presence of interstitial solutes like carbon and nitrogen are essential[50-52].

The martensite/austenite interface has been described as a misfit region containing a network of dislocation[53]. Such interfaces are mobile in nature in the presence of suitable chemical or mechanical driving forces[54,55]. During aging, the interface dislocation can be immobilized[51,52,56,58,59] by the pinning action of the segregated interstitial atoms i.e., forming "Cottrell Atmospheres"[60] resulting in a complete cessation of growth. Recent studies (Fig. 6)[61] on a medium carbon steel indicate that the carbon content at the interface may attain values of 5 to 10 at %, high enough to stop the movement of the interface.

In plate martensitic steels, the amount of 'blocky' austenite retained can be controlled by holding the sample at a temperature above or below M_s[51,52,62,63]. In these cases the amount of retained austenite increases as the temperature is increased and the time of hold extended. This is attributed mainly to carbon segregation to the dislocations at the interface. A similar phenomenon may be attributed in the case of lath martensite containing thin film retained austenite caused by the trapping of the high temperature phase between the interfaces of two adjacent laths. The bct martensite lattice is strained by the trapped

carbon which diffuses towards the interface and into the γ to an extent that time and temperature permit. The carbon atoms diffusing to the interface segregate at the dislocation present at these sites. The resulting dislocation-interstitial reaction created, produces a net force which opposes the interface movement[64].

The phenomenon of thermal stabilization may be explained as follows. The interaction of the elastic stress fields around interstitial solute atoms with that of the semicoherent interface decreases the elastic strain energy. This furnishes a driving force for the segregation of the solute atoms to the interface[54,65]. Besides, during the slow propagation of the interface at high temperatures[59,63] carbon can diffuse over long distances under the influence of the strain fields of the interface. The degree of stabilization depends on the concentration of the anchoring atoms[65] at the interface. Hence the stabilization depends on the rate of carbon diffusion at a temperature, which is lowered, at a decreasing rate, during cooling. Also the binding of the carbon atoms to the dislocation increases with the lowering of the temperature[59,65], thereby increasing the effect of thermal stabilization. However, the maximum effect of this stabilization may not be attained due to the decrease in carbon diffusion as the temperature is lowered.

Therefore it has been concluded that the observed increase in the carbon concentration at the interface occurs mainly at high temperatures in the temperature range through which cooling takes place.

2.2 Mechanical Stabilization

During the $\gamma \rightarrow \alpha'$ transformation, the growth of individual laths can be viewed as a systematic motion of the α'/γ interface. It has been observed that during such transformations, the lattice of the parent phase ahead of the transformation front contains a high concentration of structural defects, e.g., dislocations, ledges, faults, etc. (Figs. 7 and 8). These imperfections arise as a result of accommodation of strains created by the dilational and shear stresses[64,66,67].

Since the shearing of such an imperfect lattice is difficult, the parent (austenite) phase resists the continuation of the transformation[68]. The movement of the γ/α interface will thus be impeded by the presence of these defects[57,59,68].

As the transformation proceeds, plastic deformation of the parent austenite phase takes place resulting in creation of more dislocation ahead of the transformation front. Under such conditions, the continuation of the transformation process requires a continuous increase in the driving force. Since such as increase in the driving force cannot be achieved under any conditions of cooling, the reaction comes to a halt.

The presence of structural defects, e.g., dislocations,besides obstructing the movement of the interface also affects its movement indirectly because of the carbon redistribution in the austenite. The distribution generally takes place at the higher temperatures of the M_s-M_f temperature range during which carbon segregates at the dislocations thereby enhancing their immobility[55,59]. This results in making the deformation of the austenite more difficult in the presence of the shear process.

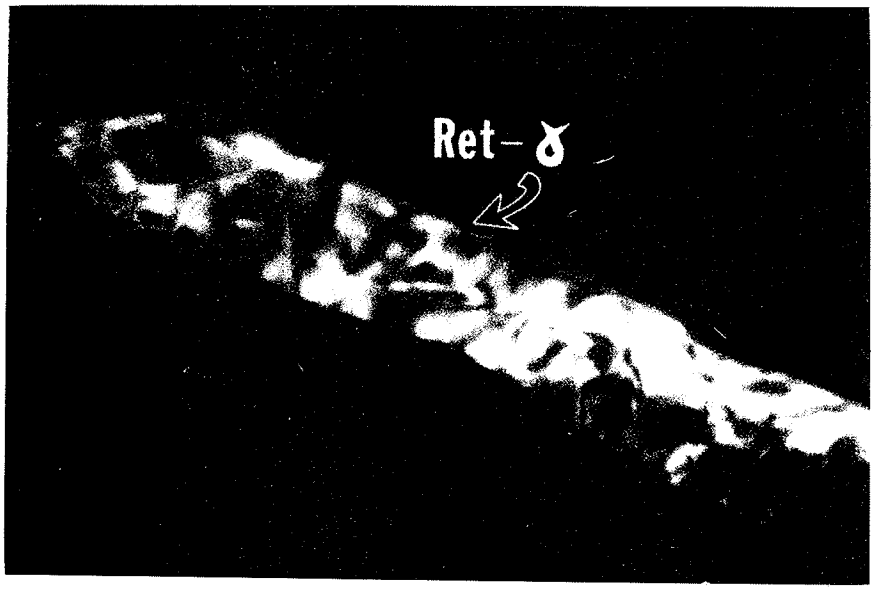

Figure 7. High magnification dark field micrographs of a region containing thick retained austenite film, show the contrast change due to defects arising from heavy deformation[64]

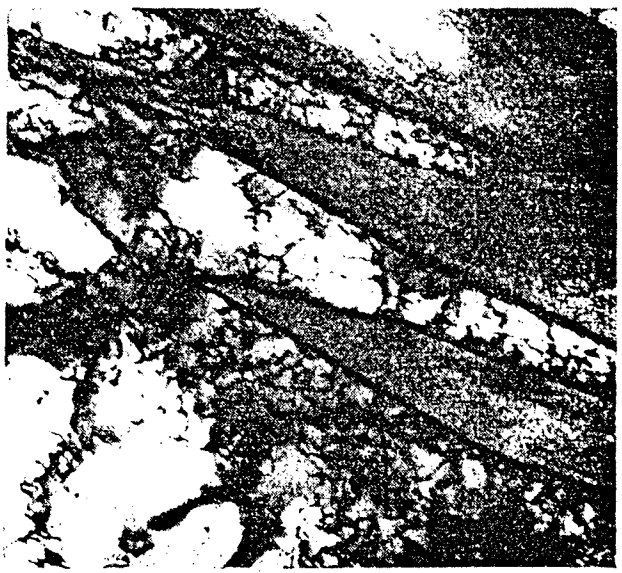

Figure 8. Dislocation surrounding martensite plates (M) in the quenched Fe-Ni-C steel[68].

Also the fast cooling rates needed for such transformation imparts a remarkably high degree of residual strains[69]. Stresses of the order of 50 ksi[70] may result due to the quenching which is about 10% of the stresses caused by the volumetric change accompanying the $\gamma \rightarrow \alpha'$ transformation. Since these residual stresses have to be accommodated they are presumed to contribute to the local stabilization of austenite[71,72].

2.3 Chemical Stabilization

The initiation and progress of the $\gamma \rightarrow \alpha'$ transformation are both controlled by the chemical and non chemical free energies of the system[73-74]. The chemical free energy depends largely on the chemical species of the phases. If variation in the chemistry of the austenite phase can be brought about by any means, then the course of the transformation is altered. Thus, changes in the alloy content (both substitutional and interstitial) of the austenite will alter the driving force required to bring about the transformation.

When a γ-solid solution of an Fe-A alloy transforms into an α-solid solution of the same composition, the chemical free-energy ΔF_{Fe-A} accompanying it is expressed by the sum of the following terms[70].

$$\Delta F_{Fe-A}^{\gamma-\alpha} = (1-x)\ \Delta F_{Fe}^{\gamma-\alpha} + x\ \Delta F_{A}^{\gamma-\alpha} + \Delta F_{M}^{\gamma\rightarrow\alpha} \qquad 2.1$$

where x is the concentration of component A in atom fraction. In the above equation, the first, second, and third terms respectively represent change in the free energy of the solvent atoms, solute (A) atoms and the mixture (solid solution) of Fe and A atoms. The first term can be estimated[70] but the second and third terms are difficult to

calculate. Despite this difficulty efforts have been made to measure these terms and they are as follows.

Thermodynamic properties of medium alloy steels have been derived[74] by assuming the phases to be ideal solutions and therefore the mixing term, i.e., $\Delta_M^{\gamma\to\alpha}$ is negligible. Furthermore it is also assumed that $\Delta S_A^{\gamma\to\alpha} = 0$[75] and thus the second term, i.e.,

$$\Delta F_A^{\gamma\to\alpha} - T\Delta S_A^{\gamma\to\alpha} = \Delta H_A^{\gamma-\alpha} \qquad 2.2.$$

Thus

$$\Delta F^{\gamma-\alpha} = (1-x)\ \Delta F_{Fe}^{\gamma-\alpha} + x\ \Delta H_A^{\gamma-\alpha}\text{[70]} \qquad 2.3$$

where $\Delta H_A^{\gamma\alpha}$ is the difference between the heats of solution of component A in α and γ solid solutions and is nearly equal to $\Delta H_A^{\gamma\alpha'}$ (α' denotes martensite). Numerical values are listed in Table 1[74-76].

Using measured values of various thermodynamic quantities, $\Delta F^{\gamma\to\alpha}$ has been related to absolute temperature T[73] viz.

$$\Delta F^{\alpha-\gamma} = 1202 - 2.63 \times 10^{-3}T^2 + 1.54 \times 10^{-6}T^3 \text{ cal/mol.} \qquad 2.3.a$$

for T = 200° - 900° k, and

$$\Delta F^{\alpha-\gamma} = 1474 - 3.4 \times 10^{3}T^2 + 2 \times 10^{-6}T^3 \text{ cal/mol} \qquad 2.3.b$$

for T = 800° - 1000°k.

These equations undergo slight modification when ferromagnetison of α iron is taken into account.

The austenite-martensite equilibrium temperature T_o is either raised or depressed depending on whether the chemical species makes

TABLE 1

Difference in Heat of Solution Between γ and α' Fe Phases[70]

Alloying Element	$\Delta W_A^{\gamma\rightarrow\alpha}$ (cal/mol)	Alloying Element	$\Delta W_A^{\gamma\rightarrow\alpha}$ (cal/mol)	Alloying Element	$\Delta W_A^{\gamma\rightarrow\alpha}$ (cal/mol)
C	8100	Cu	1280	Mo	-1360
N	5360	Zn	590	V	-2830
Mn	2440	Si	-475	P	-4180
	2700	Be	-810	Sn	-5500
Ni	1600	Al	-1300	Ti	-9000
	2500	W	-1360	Cr	1200

$\Delta H_A^{\gamma-\alpha'}$ positive or negative. The T_o term is the main factor in determining M_s.

Subsequently, a more rigorous treatment was applied to this aspect in the case of high alloy steels[77]. In this treatment the mixing term was assumed to be a regular solid solution. This led to the following equation for Fe-Ni alloys which is applicable up to 1000°k.

$$\Delta F_{Fe-Ni}^{\gamma\rightarrow\alpha} = (1-x)\ \Delta Fe^{\gamma\alpha} - x\ (-3700 + 7.09 \times 10^{-4}T^2 + 3.91 \times 10^{-7}T^3) - x\ (1-x)\ [3600 + 0.58T\ (1-\ln T)]\ \text{cal/mol} \qquad 2.4$$

The temperature, T_o, at which $\Delta F_{Fe-Ni}^{\gamma-\alpha}$ vanishes is shown in Fig. 9.

As in the case of nickel, the mixing term has been taken into consideration while calculating the free energy change in the case of alloying elements[78,79] such as carbon and nitrogen. In the case of tetragonal martensite formation, the free energy change calculations

taking into account the ordering of the interstitial atoms[80] has led to the establishment of the following equation[81].

For disordered (cubic crystals) formation, the free energy change $\Delta F^{\gamma \to \alpha'}$ was obtained by using equilibrium calculations of the α and γ phases. The result was

Fe-C system

$$- \Delta F^{\gamma-\alpha'} = (1-x)\ \Delta F_{Fe}^{\gamma\alpha} - x\ (5552 + 1.65\ RT) - RT\ [x \ln \frac{x}{1-2x} - x \ln \frac{x}{3(1-2x)}] - RT\ \frac{3x^2}{1-x}\ \{[1-\exp(\frac{-1032}{RT})]^2\ [2-\exp(\frac{-1032}{RT})] + \frac{2064}{RT} \exp(\frac{-1032}{RT})\} + 1.8 \times 10^4\ (\frac{x}{1-x})^2 \text{ cal/mol} \qquad 2.5$$

Fe-N system

$$- \Delta F^{\gamma-\alpha'} = (1-x)\ \Delta F_{Fe}^{\gamma-\alpha} - x\ (5360 + 1.92\ RT) - RT\ [x \ln \frac{x}{1.2x} - x \ln \frac{x}{3(1-2x)}] - RT\ \frac{3x^2}{1-x}\ \{[1-\exp(\frac{-1180}{RT})]^2\ [2-\exp(\frac{-1180}{RT})] + \frac{2360}{RT} \exp(\frac{-1180}{RT})\}\ 1.8 \times 10^4\ (\frac{x}{1-x})^2 \text{ cal/mol.} \qquad 2.6$$

In the case of tetragonal crystals in which interstitial atoms take an ordered arrangement, the following relation holds[82].

$$- \Delta F^{\gamma \to \alpha'} = - \Delta F^{\gamma-\alpha} - F \qquad 2.7$$

$$F = \frac{1}{3} N \phi (\frac{x}{1-x})^2 (1-s^2) + NRT \{\frac{1}{3} \frac{x}{1-x} (2s+1) \ln[\frac{1}{3} \frac{x}{1-x} (2s+1)] + [1 - \frac{1}{3} \frac{x}{1-x} (2s+1)] \ln [1 - \frac{1}{3} \frac{x}{1-x} (2s+1)] + \frac{2}{3} \frac{x}{1-x} (1-s) \ln [\frac{1}{3} \frac{x}{1-x} (1-s)] + 2 [1 - \frac{1}{3} \frac{x}{1-x} (1-s)] \ln [1 - \frac{1}{3} \frac{x}{1-x} (1-s)]\} \qquad 2.8$$

where N is the number of Fe atoms and s is the long range order parameter for the arrangement of interstitial atoms (zero for cubic crystals). The interaction energy between interstitial atoms in the lattice ϕ, has been estimated to be 3.74×10^{-2} ergs for both Fe-C and Fe-N alloys assuming that the decrease of the energy due to ordering of the interstitial atoms in the tetragonal crystal balances the increase of the elastic energy due to tetragonal distortion. Equation 2.8 and eq. 2.3.b therefore yield $-\Delta F^{\gamma\rightarrow\alpha'}$ as a function of x and T. Fig. 10[81] indicates temperature T_o at which $\Delta F^{\gamma-\alpha}$ becomes zero. The M_s versus solute concentration curve for nitrogen containing steels run almost parallel to and lies below the T_o curves (by about 200°C) obtained from the above relations $\Delta F^{\gamma-\alpha'} = 0$. However the $\Delta F^{\gamma-\alpha'}$ values obtained at M_s temperature using equations 2.7 and 2.8 was found to be 300 cal/mol.

This value corresponds to the total amount of non chemical free energies which also constitute the driving force for these reactions. Fig. 9 shows the observed values of M_s temperatures as a function of nickel content[77]. T_o was determined by using the condition $\Delta F^{\gamma-\alpha'} = 0$. Calculations showed that the driving force at 27 atom % nickel is 350 cal/mol and that the driving force is higher or lower than this value depending on whether the nickel is more or less than 27 atom %. Fig. 11 indicates the M_s curves for various concentration of Fe-base binary alloys[82]. It can be seen that the alloying elements that lower T_o generally decrease M_s temperatures also.

Estimated effects of alloying elements on M_s temperature in alloys with more than three elements indicate that the effects of C and N are additive relative to each other but not so with those of other substitutional elements[83,87]. The effects of substitutional elements can be

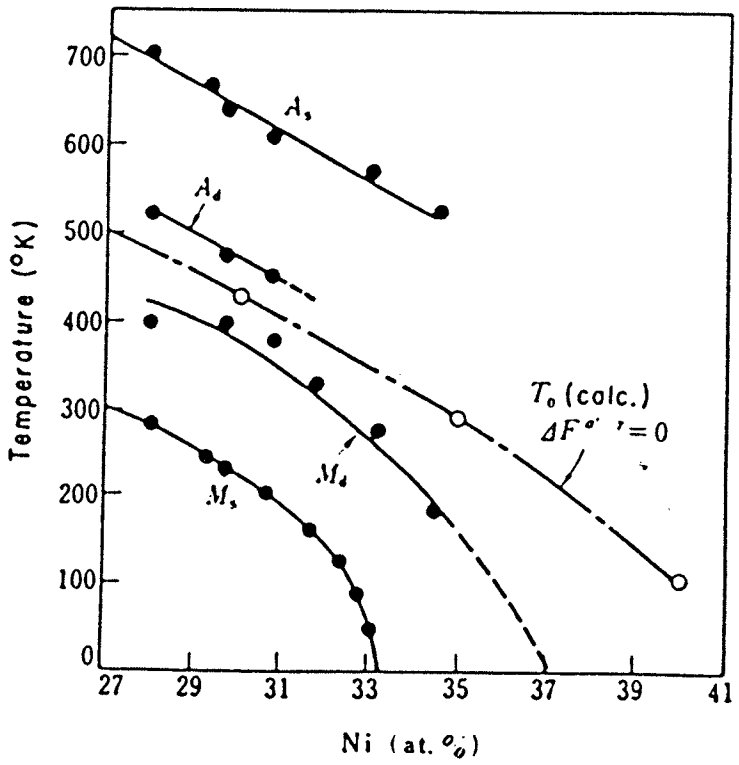

Figure 9. Transformation Temperature of Fe-Ni alloys (with Nickel contents higher than 27%[11].

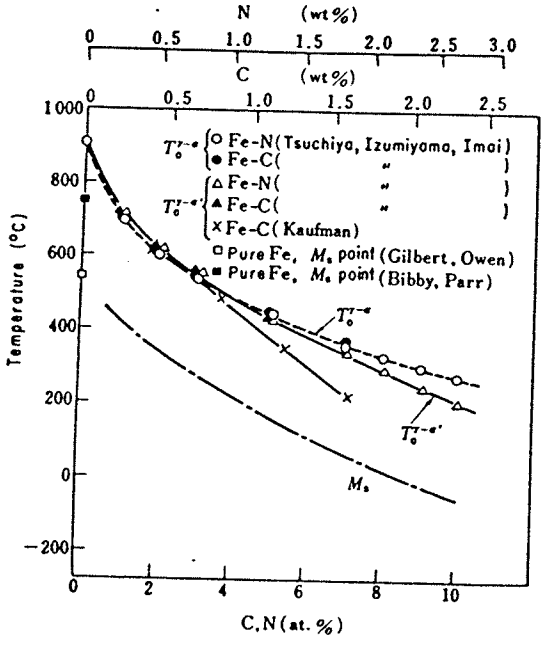

Figure 10. M_s and T_0 Temperatures of Carbon and Nitrogen Containing Steels[81]

mutually additive excepting a few cases[88]. Table II shows the variation of M_s temperatures with the addition of a third element to Fe-Ni alloys. In the case of Fe-C alloys variation of the transformation with nickel additions is shown in Fig. 12[89]. Reports on the nickel equivalent of the fourth elements in the case of 18/8 stainless steels are as follows: $S_i = 0.45$, $M_n = 0.55$, $C_n = 0.08$, C = 27, and N = 27[90].

For $\gamma \rightarrow \varepsilon$ transformation in these alloys, the fourth element elevates or suppresses the transformation temperature depending on whether it decreases (e.g. silicon) or increases (e.g. carbon) the stacking fault energy[91].

From data available so far, it can be concluded qualitatively that addition of any alloying element other than Cobalt, will suppress the M_s temperature and the extent of such suppression can be enhanced by an increase in the addition of the alloying elements.

2.4 Stabilization of Austenite due to Austenite Grain Size Effect

It has been concluded from several experimental observations that the inhibition of the $\gamma \rightarrow \alpha'$ reaction is enhanced by reducing the size of austenite grains. Some of the more important observations made in this regard are depicted in Figs. 13 to 15, and Table 3. The reasons suggested so far, to explain this phenomenon, are as follows.

Grain boundaries, despite being defect structures and hence preferential sites for martensite nucleation, serve to inhibit martensite transformation. This is because the growth of the martensite crystal is considerably difficult at the grain boundaries. The grain boundary atoms being relatively free from restriction by neighbouring atoms (unlike atoms in the grain body) tend not to participate in the

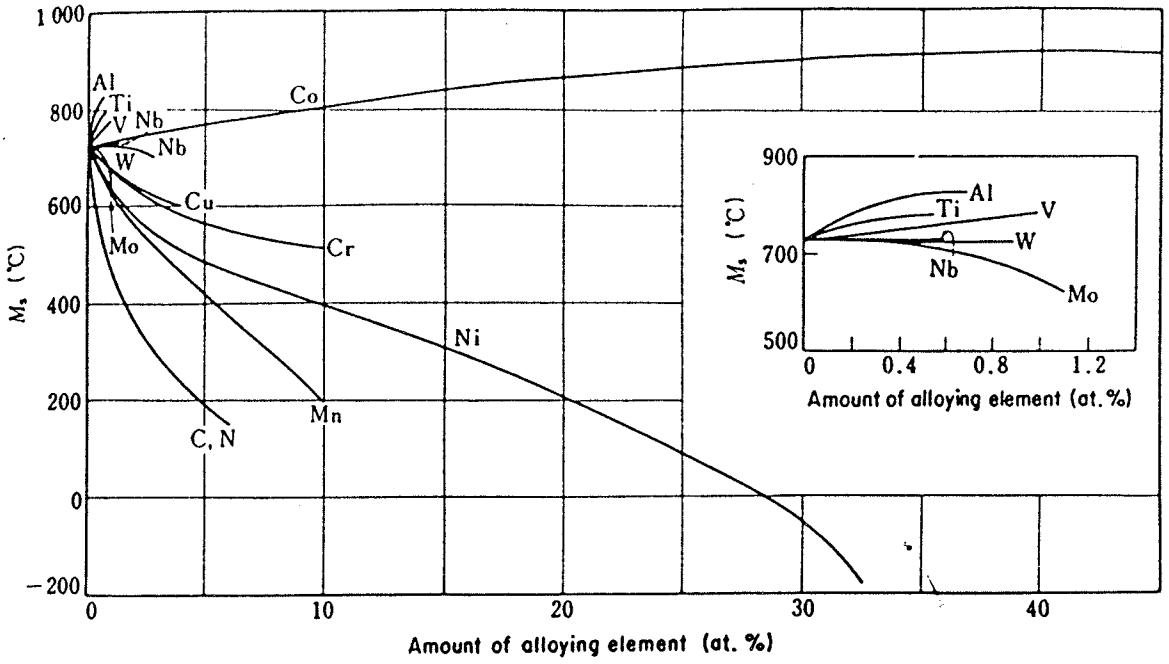

Figure 11 M_s Temperature of Fe-base Binary Alloys[82]

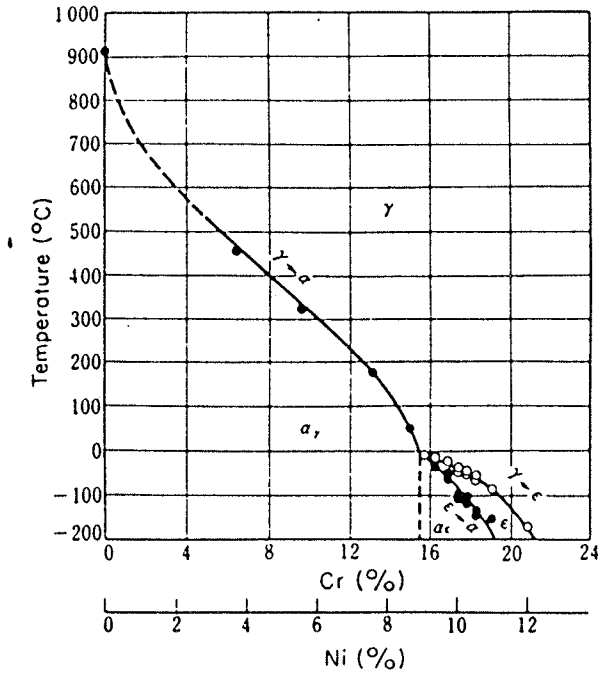

Figure 12 Transformation Temperatures of Fe-Cr-Ni Alloys (Cr: Ni = 5:3)[89].

TABLE 2

Effect of Third Elements on the Transformation Temperatures of Fe-Ni Alloys[80]

Mother Alloy Fe-Ni(%)	Ti		V		Nb		Cr		Mo		W		Mn		Co		Ni		Cu		Al		Si	
	M_s	A_s	M_s	A_s	M_s	A_s	M_s	A_s	M_s	A_s	M_s	A_s	M_s	A_s	M_s	A_s	M_s	A_s	M_s	A_s	M_s	A_s	M_s	A_s
22.5%	↷		↷		↷		↓	↓							↑	↑	↓	↓			-		↷	
27-30%					↷		↓		↓		↓		↓								-		↓	
18, 30%			↑	↓			↓	↓	↑	↓			↓	↓	↑	↑			↓	↓	↓	↓	↓	↑

Key: ↓ fall; ↑ rise; ↷ rise and then fall; - no change.

co-ordinated movement (shearing of the parent lattice) so essential for the growth of the martensite nucleus[70]. Besides this, the lattice defects in the vicinity of the grain boundary can migrate to the boundary. Thus the number of potential nucleation sites is reduced[70].

It may be mentioned however, that despite the numerous investigations made in this area a rigorous explanation of the reasons behind this observed phenomenon is not available. The best explanation put forward so far is from a study of the dependency of the nucleation rate of martensite as a function of austenite grain size[109] in the case of a Fe-24 Ni - 3 Mn steel. It showed that the isothermal nucleation rate decreases as the austenite grain size is reduced which may be understood as follows.

The number of embryos existing at time t per cm^3 of the alloy is given by

$$N_t = (n_i + pf - N_v)\ (1-f) \qquad 2.9$$

where p is autocatalytic factor, i.e., the number of embryos generated per cm^3 of martensite formed. This parameter is not sensitive to the grain size of austenite but increases with decrease in the reaction temperature, n_i, is the number of embryos initially present per cm^3 of austenite. It is independent of the austenite grain size f, is the volume fraction of martensite formed N_u is the number of martensite plates per unit volume of the specimen.

The rate of activation of embryos per cm^3 of the alloy can be expressed as[106]

$$\frac{dN_u}{dt} = n_t\ \nu\ \exp\ [^{-\Delta W}a/RT] \qquad 2.10$$

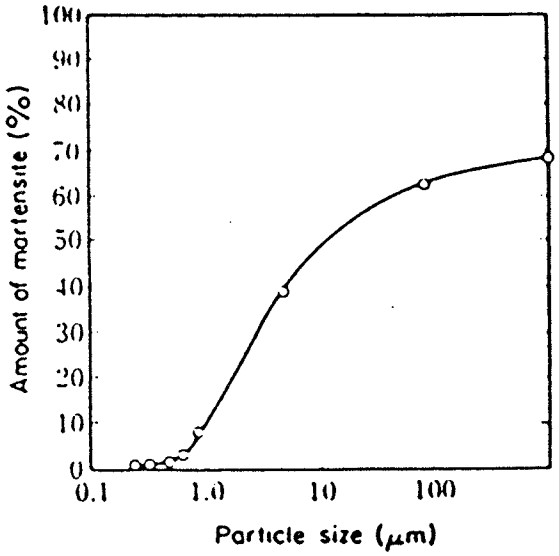

Figure 13. Amount of martensite as a function of particle size of powders, for Fe-27.4 Ni alloy powder quenched to room temperature[103].

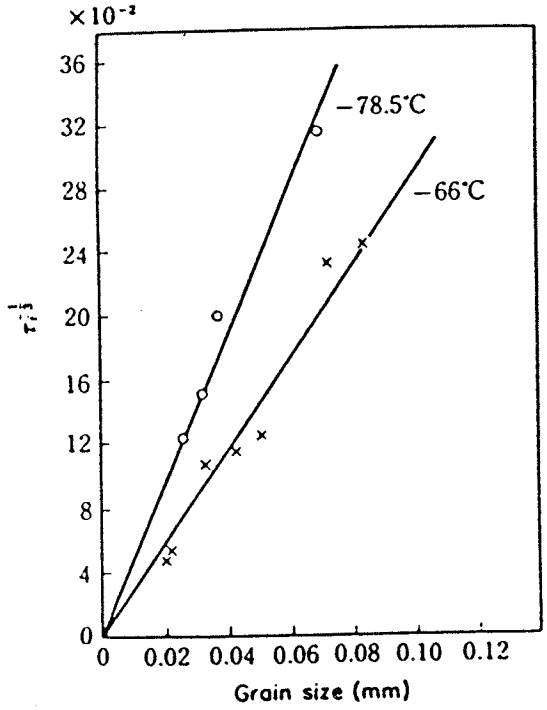

Figure 14. Effect of austenite grain size on incubation period (in seconds) of martensite for a Fe-26 Ni - 2Mn alloy[107i].

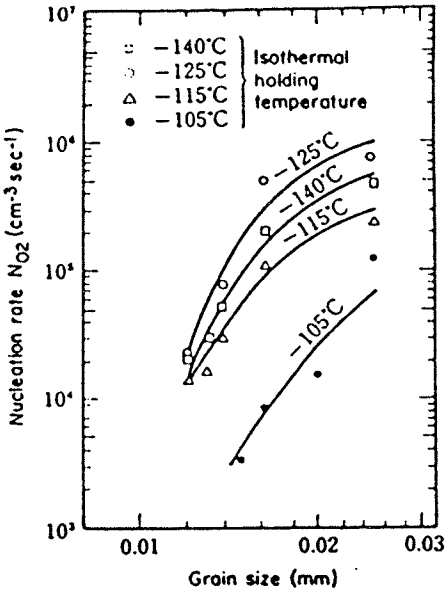

Figure 15. Effect of austenite grain size on the nucleation rate in a Fe-24 Ni - 3Mn alloy[109].

where ν is the lattice vibrational frequency (10^{13} per sec)

ΔW_a, is the increment of free energy required to activate Avogadro's number of embryos which include the autocatalytic embryos in addition to the initial ones.

From eqs. 9 and 10

$$\frac{dN_v}{dt} = (n_v + p\ f - N_v)\ (1-f)\ \nu \exp\ [^{-\Delta W}a/RT]$$

the rate of isothermal nucleation is defined as

$$\dot{N} = \frac{1}{1-f}\ \frac{dN_v}{dt} \qquad 2.11$$

Therefore $\dot{N}\ (1-f) = (n_v - p\ f - N_v)\ (1-f)\ \nu \exp\ [^{-\Delta W}a/RT]$

or $$\dot{N} = (n_i + p\ f - N_v)\ \nu \exp\ [^{-\Delta W}a/RT] \qquad 2.12$$

TABLE 3[90]

Stabilization of austenite by fineness of grains in Fe-31.5% NI-0.02% alloy[90]

Average Austenite Grain Diameter, μ	ASTM Grain Size	Retained Austenite at -195 C, %
60	5.5	5
9.4	11	12
0.6	19	74

Hence, for a constant value of f, $\dot{N}$ will be a function of N_v where $N_v = f/\bar{v}$, $\bar{v}$ being the mean volume per martensite plate[109]. $\bar{v}$ can be estimated using Fullman's equation[111], i.e.,

$$\bar{v} = \pi^2 f/8\ell^{-1}N_A \qquad 2.13$$

where N_A is the number of crystals per unit area of specimen cross-section and ℓ^{-1} is the mean value of the reciprocal of the length of the martensite plate.

Since N_v, for a fixed value of f will increase as the grain size is reduced, $\dot{N}$ will decrease. Consequently higher nucleation events will have to occur to produce the same amount of martensite in the fine grained alloy. The time for the formation of 0.2% martensite corresponding to various reaction temperatures and embryo radii for a Fe-24Ni-3Mn alloy is shown in Figure 16[109]. The activation energy ΔW_e for the spreading of the interface according to this model is expressed as

$$\Delta W_e = 4 \times 10^{-2} (a/A)^{\frac{1}{2}} [3 \sigma r_e^{3/2} + \Delta g^{\gamma-\alpha} (\alpha/A)^{\frac{1}{2}} r_e^2] \qquad 2.14$$

ergs/embryo

where σ is the interfacial energy in ergs/cm^2, A is the strain energy factor (2.1 x 10^{10} dynes/cm^2), r_e is the radius in cm of the largest embryo and provides a measure of the "strength" of the most potent nucleation sites. $\Delta g^{\gamma-\alpha}$ is a function of temperature and composition[114].

Figure 16 indicates that if the most potent embryos are smaller than a certain size (210 A° in this case), there exists a C curve relationship between $t_{0.2}$ and the reaction temperature. Under such conditions isothermal transformation without prior althermal transformation is not only accessible, but quenching to very low temperatures

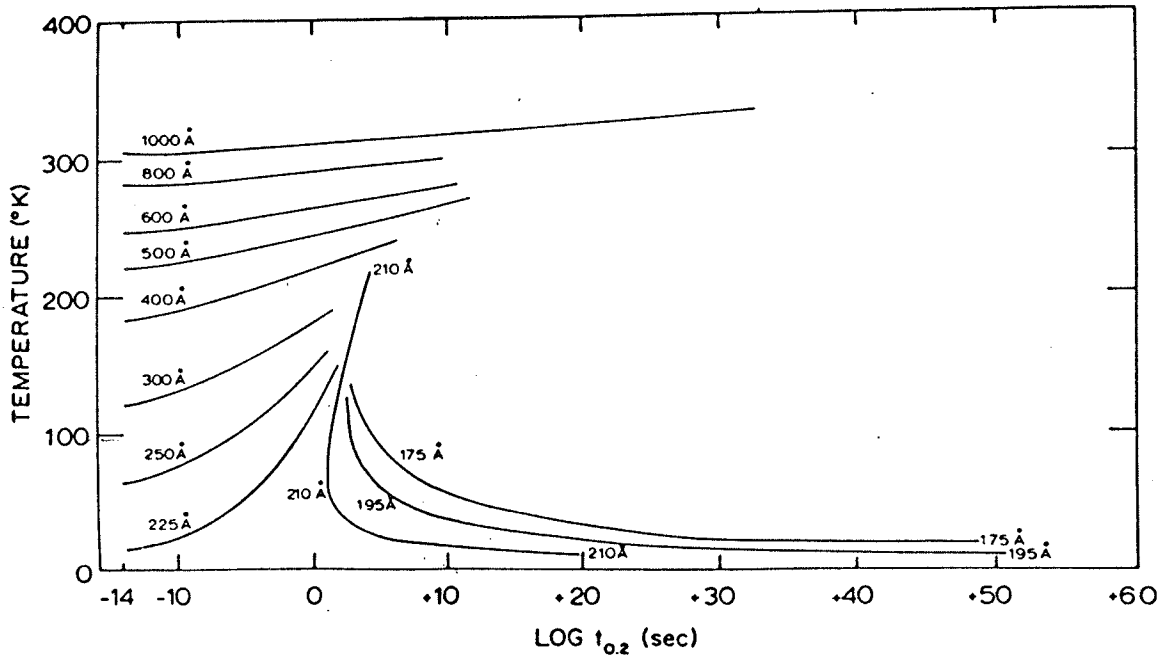

Figure 16 Calculated time for 0.2% Martensite transformation as function of reaction temperature for various embryo sizes (indicated in A°) in a Fe-24Ni-3Mn alloy with austenite grain size of 0.025 mm[109].

can suppress the transformation completely. On the other hand with embryo sizes larger than a certain size (which is 225 A° in the study being referred to), the $t_{0.2}$ curves do not have the C shape and tend to become horizontal at times approaching zero and high temperatures. Each of these horizontal curves represent insuppressible transformation on cooling and represents a true athermal M_s temperature for the given embryo size.

The curves which slope upwards to higher temperatures at larger times signify that even for embryos larger than the size at which they no longer have the C shape, isothermal transformation can take place during holding above the respective M_s temperature. For the case cited here, this phenomenon is quite pronounced in the embryo size range of 225-400A°. In many cases one cannot make an experimental separation between althermal and very rapid isothermal nucleation. In fact, the distinction between althermal and isothermal kinetics is purely empirical and althermal transformation can be regarded as rapid isothermal reaction[115].

The change of the C curves in Fig. 16 to transformation curves with insuppressible features as embryo size increases is caused by an accompanying decrease in ΔW_e a value of zero is less. In other words the condition for a true M_s temperature is $\Delta W_e \leqq 0$. For this condition to be satisfied the bracketed quantity in equation 2.14 has to be equal to or less than zero, i.e.,

$$r_e (\Delta g)^2 \geqq g\sigma A \qquad 2.15$$

Therefore the M_s temperatures are more likely to be encountered than full C curve behaviour with increasing size of the embryos/and or greater the driving force. When the above condition is not satisfied a

full C curve results, although it may not be detectable if the curve happens to lie too far to the right of the time axis. Thus if for any given case a full C curve, detectable or otherwise exists, there will be no insuppressible M_s even at the lowest possible temperatures.

In view of the above observation it is suggested that the inhibition of $\gamma \rightarrow M$ transformation in fine grained austenite with similar chemical composition and some free energy change ($\Delta g^{\gamma-\alpha}$) is a consequence of the above stated condition for insuppressible M_s being not satisfied. Under the constraints of identical chemical composition and free energy change, this is possible if any only if the interfacial free energy term (σ) for the nucleation of martensite in fine austenite grain is extremely high compared to that in the coarse grain.

Lattice defects in the vicinity of the grain boundary migrate to the boundary and disappear[70]. For fine austenite grains this phenomenon will be very pronounced because of the higher grain boundary area that is available per unit volume of the grain body. The resultant reduction of defect and grain body interfaces will cause an increase in the interfacial free energy term (σ) thereby resisting the transformation process.

CHAPTER III

GENERAL CONSIDERATIONS

Various austenite stabilization mechanisms that may operate during the cooling of steels have been discussed in Chapter 2. In this chapter, different aspects pertaining to austenite retention in intercritically annealed low alloy-low carbon steels are considered. Retained austenite morphologies along with the underlying factors that contribute to their retention are reviewed. Also, austenite formation and factors such as starting microstructure that influence its kinetics are discussed. Finally, a choice is made about the starting microstructure which may yield higher than usual amounts of γ_R on intercritical annealing.

3.1 Various Aspects of Austenite Retention in I.C. Annealed Dual Phase Steels

Retained austenite (γ_R) in intercritically annealed dual phase steels can be classified into three categories on the basis of their morphologies. They are a) interlath type[116], b) capsulated type[117-119] and c) isolated type[22,24] as shown in Fig. 17.

The interlath type of γ_R is found in the form of thin continuous films separating adjacent martensite laths as shown in Fig. 17(a). This type of γ_R is generally observed when low or medium carbon steels are quenched from the austenitization temperatures[61] (above A_3 temperatures) and is seldom observed in dual phase steels unless quenched from high intercritical annealing temperatures ($\sim$ 825°C) after relatively long holding times ($\sim$900 sec)[116]. The retention of this type of austenite in

Figure 17(a)

Figure 17b)

For a low carbon-low alloy steel which has been water quenched after annealing at 825°C for 15 minutes, 17(a) shows the bright field micrograph of a martensite nodule. 17(b) shows this austenite imaged as bright streaks in a dark field micrograph.

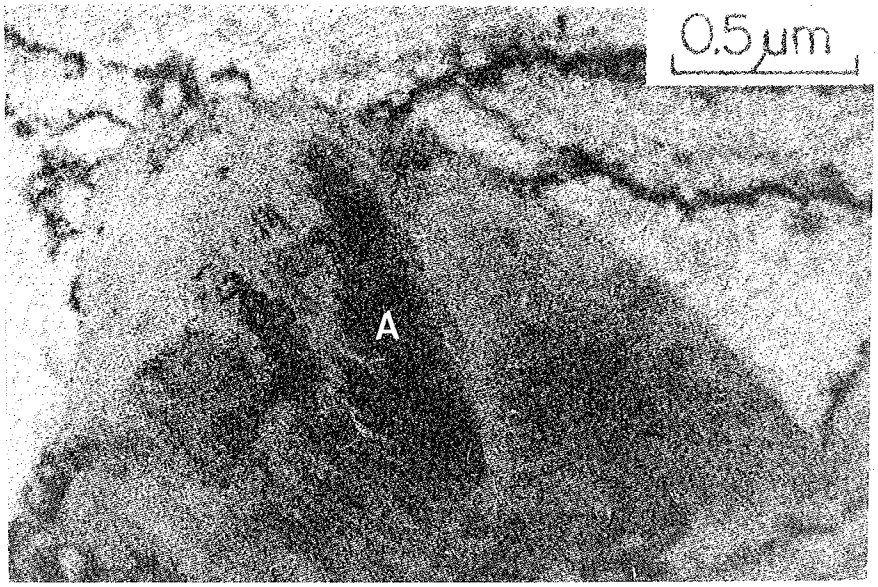

Figure 17(c)

Bright field micrograph of capsulated type retained austenite, (marked A)[31].

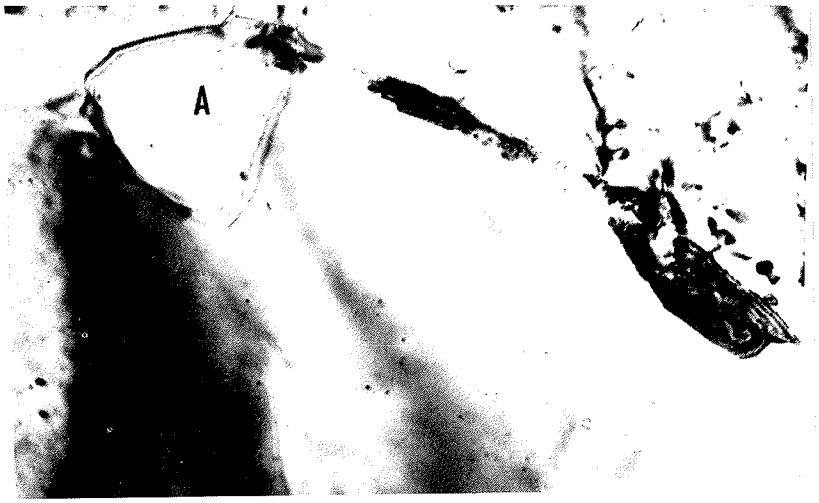

Figure 17(d)

Bright field micrograph of isolated type retained austenite (marked A) surrounded by ferrite[43].

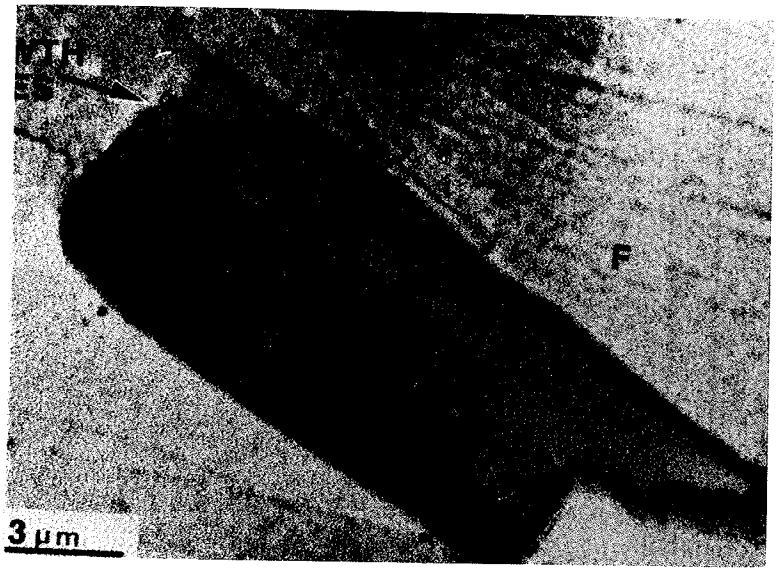

Figure 17(e)

Bright field micrograph of isolated type retained austenite (marked A) surrounded by ferrite[22].

low and medium carbon steels has been investigated in considerable detail. These studies have attributed the retention of this type of γ_R to the combined effects of chemical, mechanical and thermal stabilization of the parent austenite phase[61].

The capsulated and isolated type of γ_R are more commonly observed in I.C. annealed dual phase steels. Capsulated type of γ_R has no particular shape and is found inside martensite particles (Fig. 17c) Isolated type of γ_R is observed at ferrite grain boundaries in the form of discrete islands.

The surrounding martensite of the capsulated type, generally consists of microtwins which is characteristic of martensite formed from highly alloyed austenite. It has therefore been suggested that such austenite particles are stabilized due to the localized enrichment of the parent phase by carbon and/or other alloying elements. It may be mentioned that austenite retained in dual phase steels is stable even at temperatures as low as liquid Helium temperatures[22,120] (-269°C). These experimental observations support the contention that the retention of capsulated austenite particles at such low temperatures must be due to a very high degree of enrichment of the austenite by carbon and/or other alloying elements. It is however not understood as to how such a high degree of enrichment can be achieved. Such suggestions therefore call for the microanalysis of the chemistry of capsulated type of γ_R particles.

Investigation of the chemistry of isolated type γ_R particles has revealed considerable segregation of carbon and manganese[22,43,120]. Although these elements are known to stabilize austenite by depressing the M_s temperature, the level of enrichment is not sufficient to account

for the suppression of M_s temperature even up to room temperatures (not to mention the liquid helium temperature) even if complete partitioning of carbon and significant partitioning of manganese occurs. It must be noted that typical annealing times corresponding to which austenite is retained in these steels are too short to allow such partitioning. Obviously the retention of isolated type γ_R particles and most likely even capsulated type γ_R particles cannot be solely attributed to chemical stabilization. Hence other stabilization mechanisms namely

i) Mechanical stabilization

ii) Thermal stabilization

iii) Austenite particle size stabilization

will be considered to account for the high stability shown by the γ_R particles.

It is quite unlikely that mechanical stabilization plays a significant role. Such an inference is based on the following arguments. For mechanical stabilization to be operative, it is necessary that the parent austenite lattice be deformed (Figs. 7 and 8). Under such conditions the shearing of the lattice becomes increasingly difficult resulting in increased resistance to the growth of martensite crystals. The growth of individual martensite laths which involves the movement of the austenite/martensite interface is impeded by the presence of the defects such as dislocations in the parent phase. In addition to the direct obstruction to the movement of the interface, there is also an effect of carbon re-distribution in the deformed austenite. This happens at higher temperatures in the M_s-M_f temperature range where the interstitial atoms segregate to the dislocations in the austenite thereby increasing the strength of the parent lattice. The resistance

to shearing of the parent lattice is thus enhanced. Electron-microscope studies of the substructure of both isolated and capsulated type of retained austenite particles have so far not revealed the presence of any dislocation network[4,5,8-10,22,38,112]. The absence of such defects would at least suggest that mechanical stabilization is not playing a significant role.

Thermal stabilization, as described earlier, is caused by the cessation of the movement of the austenite-martensite interface which is considered to be a dislocation network. The cessation is brought about by the pinning action of the interstitials such as carbon and nitrogen atoms. Such stabilization processes are normally detected by high precision microanalysis (such as Convergent Beam Electron Diffraction and Atom Probe Analysis)[64] of the austenite/martensite interface which would detect a very high concentration of carbon or nitrogen at the interface. For such a stabilization mechanism to be operational one of the requirements is the presence of the martensite/austenite interface. In the case of isolated type γ_R particles such interfaces are absent, hence it is very unlikely that thermal stabilization plays a role in retaining these particles. In the case of capsulated type particles, such a mechanism can at best be regarded as only a possibility. Since microanalysis data of the austenite/martensite interface is not available.

The γ_R particles in dual phase steels have a unique feature irrespective of their morphologies. Their size usually ranges from a fraction of a micron to about 2 microns[22,43]. Since the size of the austenite grains also affects the stability of this phase as has been discussed in section 2.4, it has been suggested that the fine size of

these austenite particles also contributes to their retention at liquid helium temperatures[22,120].

Therefore the observed stability of both capsulated as well as isolated type of γ_R particles in dual phase steels has been attributed to the joint effects of austenite particle size stabilization and chemical stabilization.

During post annealing cooling, the isolated type of γ particles undergo a reduction in size. It is due to the formation of pro-eutectoid ferrite along the austenite/ferrite interface as the temperature drops within the $\alpha + \gamma$ region of the Fe-C equilibrium diagram[121]. Under such conditions it is expected that the interface on the austenite side will be enriched by the carbon atoms which are rejected by the pro-eutectoid ferrite into the austenite in the immediate vicinity of the austenite-ferrite interface. Similar enrichment of substitutional alloying elements like manganese will be insignificant due to lack of sufficient time for these elements to diffuse through any measurable distance in austenite[122]. Due to such enrichment, it is expected that austenite will be retained in the form of a rim around the martensite particle. However retained austenite of such morphology has not been observed in any investigation so far. This suggests that chemical enrichment of austenite particles through the movement of the austenite/ferrite interface in the process of cooling is not significant enough to cause their retention. However the reduction in the size of the austenite particles can cause its retention if the austenite particle size to start with, i.e. prior to cooling, is not large and/or the cooling rate is slow enough to allow a substantial amount of austenite to transform to ferrite at the austenite-ferrite interface[35].

Thus it is recognized that if the cooling rate is fast there will be no effective size reduction of isolated austenite particles and hence very little chance of their retention. The bulk of the austenite retained under fast cooling conditions can therefore be related to the presence of capsulated type of γ_R particles[35]. On the other hand the isolated type of γ_R particles will constitute the bulk of γ_R content in the case of slow cooled specimens and thus may be explained as follows. With a decrease in the cooling rate from the intercritical temperature, the average size of the isolated γ_R particles at temperatures just above M_s is reduced since the ferrite/austenite interface will move through a greater distance. As a result, more of the isolated austenite particles will experience the effects of size stabilization. Therefore, it is suggested that any increase in the volume fraction of γ_R in slow cooled specimens over that of fast cooled one will be caused by the increase in the volume fraction of isolated type of γ_R particles.

Although the observed stability of γ_R particles is considered to be due to the joint effects of chemical and austenite particle size stabilization, it has been shown in Appendix 1 that at least in the case of isolated γ_R particles, the effect of size stabilization has an overriding influence. In the case of capsulated type of γ_R particles, however it is not possible to evaluate the relative influence of each of these stabilization mechanisms due to the non availability of any quantitative data on their chemistry.

Thus it is concluded that in order to increase the amount of austenite that can be retained in dual phase steels, it is desirable to choose conditions that will yield large amounts of fine austenite particles not capable of undergoing transformation during subsequent

cooling. For identifying such conditions some aspects of austenite formation will now be considered in the following subsection.

3.2 Some Basic Features of Austenite Formation During I.C. Annealing of Dual Phase Steel

Austenite formation is a nucleation and growth type of reaction process and the reduction in the average size of austenite particles is brought about by

i) increasing the nucleation rate of austenite and/or

ii) inhibiting the growth of the nucleated austenite

This is due to the fact that the size of the product phase in such type of reactions is a function of its nucleation and growth kinetics.

It is well known that the basic pre-requisite for the formation of austenite is the presence of readily available sources of carbon supply in the form of carbide particles[123]. Also it has been observed that when carbide particles are present at ferrite grain boundaries, the nucleation rate is increased very significantly[124]. This is attributed to the creation of triple junctions in the vicinity of the carbide/grain boundary interface as shown in Fig. 18, which results in the lowering of the interfacial energy term in the equation given below.

$$\Delta G_{het} = - V\Delta G_v + A\eta + V\Delta G_s - \Delta G_D \quad [125] \qquad (3.1)$$

where ΔG_{het} is the free energy change associated with the heterogeneous nucleation of austenite

ΔG_v is the change in the volume free energy per unit volume of austenite formed

η is the surface free energy per unit area of the interface created by the austenite that is formed.

A is the total surface area of the interfaces created by the austenite

ΔG_s is the change in the misfit strain energy per unit volume of the austenite formed

ΔG_D is the change in the free energy as a result of the elimination of a defect

V is the volume of the austenite formed

Experimental observations of the microstructure of I.C. annealed low carbon-low alloy steel indicate that austenite preferentially nucleates at carbide particles situated at one of the following positions[126].

a) ferrite/pearlite interface

b) pearlite/pearlite interface

c) ferrite/ferrite interface

In view of the above discussion, it is desirable that the starting microstructure satisfy the following conditions so that more austenite can be retained in the process of I.C. annealing.

1) A large number of potential sites for austenite nucleation as stated earlier in this section, be present

2) It must have microstructural features that will inhibit the growth of the nucleated austenite particles.

It has been suggested recently[127,128] that the growth of austenite particles during I.C. annealing is significantly restricted by the presence of martensite lath boundaries (MLB). A starting microstructure consisting of martensite or more preferably tempered martensite seems to satisfy the above conditions because both these structures will provide numerous carbide particles which in turn will create triple junctions in

conjunction with the lath boundaries. Therefore a starting microstructure of martensite and tempered martensite was chosen for the present study. The conventional ferrite + pearlite starting structure was also considered to investigate the effects of starting microstructure on austenite retention. Since annealing parameters such as time and temperature of annealing influence the kinetics of austenite formation, their effects on austenite retention was also studied.

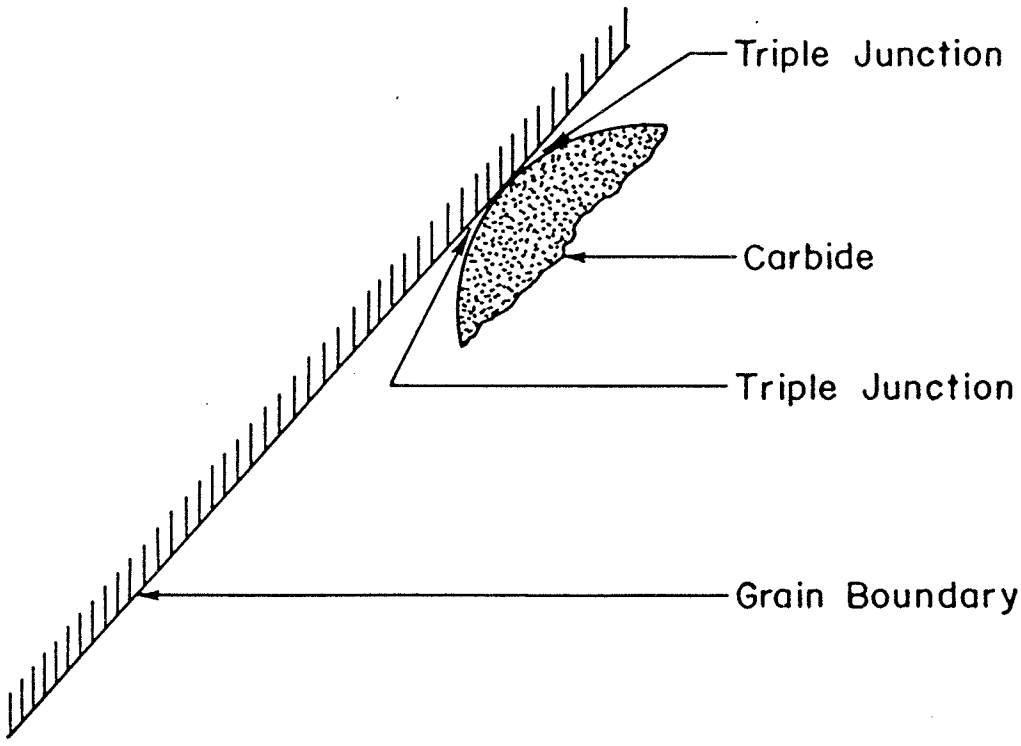

Figure 18 Highly magnified schematic view of the microstructural site at which austenite nucleates perferentially.

CHAPTER IV

EXPERIMENTAL PROCEDURES

A commercial grade line pipe steel (composition as a given in Table 4) supplied by the Interprovincial Steel and Pipe Corporation Ltd., Regina, Canada was used for this study. As received microstructure of the plate is shown in figure 19.

TABLE 4

Composition in Weight Percent	
Carbon	0.071
Manganese	1.63
Silicon	0.11
Copper	0.34
Nickel	0.07
Chromium	0.06
Niobium	0.024
Molybdenum	0.038
Tin	0.010
Sulphur	0.018
Phosphorus	0.012

4.1 Material Processing

The as received 11.5 mm thick plates were hot rolled to a thickness of 6 mm at 800°C in eight passes of equal reduction. Intermediate annealing between passes was carried out at 900°C for 6 minutes.

4.2 Heat Treatment to Obtain Various Microstructures

Various steps involved in the processing of the plates to obtain different starting microstructures are indicated in the following flow sheet.

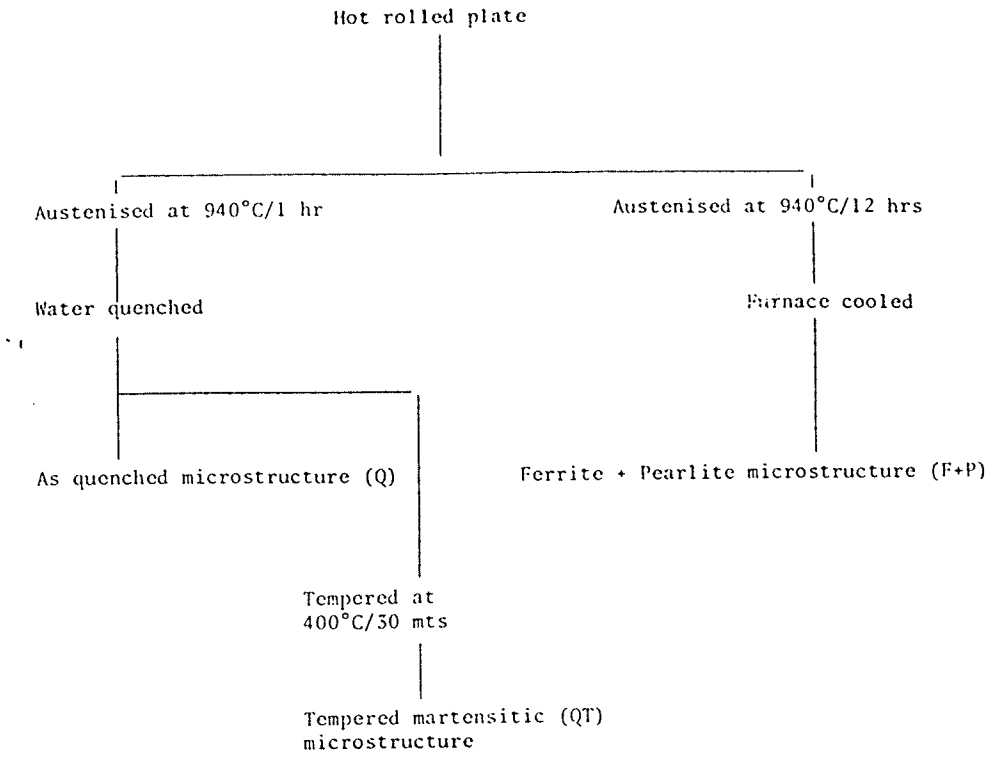

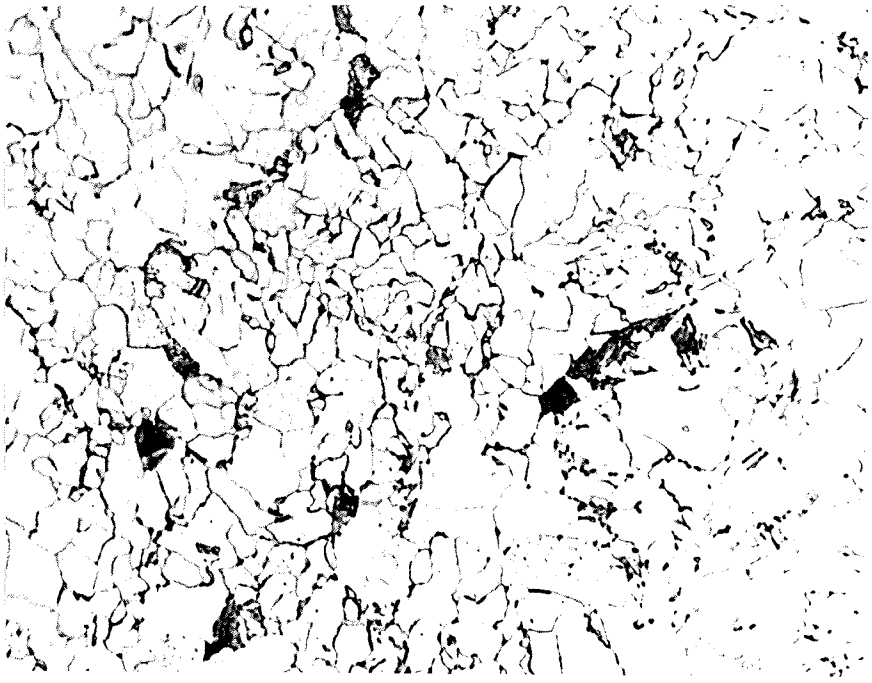

Figure 19. Micrograph of the line pipe steel in "as received" condition shown pearlite (dark) and ferrite (light) phases. Note that pearlite besides being in the form of large grains also appear at ferrite grain boundaries. [2% Nital etched].

One set of the hot rolled plates was austenitized at 940°C for one hour followed by water quenching to obtain the as quenched starting structure (Q). The other set of hot rolled plates was austenitized at 940°C for 12 hours and then slow cooled in the furnace to produce the conventional ferrite and pearlite (F+P) starting. These plates were held at the austenitizing temperature to minimize banding in the starting microstructure. Tempered (QT) microstructure was produced by tempering the tensile samples machined from some of the as quenched plates. The heat-treatment consisted of holding these samples at 400°C for 30 minutes in a argon atmosphere to avoid decarburization.

4.3. Tensile Samples

These samples were machined prior to the I.C. annealing treatment to avoid the possibility of DIMT of any austenite that may be retained after the heat treatment. The machined specimens had a thickness of 3 mm, gauge length of 12.7 mm and a gauge width of 4.5 mm.

4.4. Intercritical Annealing

The heat treatments of the tensile samples with Q, QT and F+P starting structures were carried out in a salt bath furnace. Temperatures chosen for annealing in the $\alpha + \gamma$ region of the Fe-C equilibrium diagram were 732°C, 762°C, 792°C and 818°C. A_1 and A_3 temperatures of the steel as calculated by using the appropriate relation[129] were 720°C and 864°C respectively. Post annealing cooling was done in still air (approximately at the rate of 5°C/second). A few samples were quenched in an oil bath at 50°C from 752°C and 818°C. Samples with QT starting

structure were annealed for 1, 2 and 3 minutes at various annealing temperatures. Samples with other starting microstructures were annealed for 3 minutes only at various temperatures. Short holding times were chosen to avoid significant growth of the nucleated austenite.

4.5 Measurement of Retained Austenite Volume Fraction

The volume fraction of this phase was measured by x-ray diffraction [130], details of which are described in Appendix 2. Since the austenite retained after such I.C. annealing treatment is in the form of fine particles (their diameters ranging from submicrons to a couple of microns) it was felt that x-ray analysis would give the most accurate results.

The technique consisted of finding the ratio of the areas under one austenite and one ferrite peak. This ratio is then multiplied to the inverse ratio of the respective theoretical relative intensity factors.

The tests involved irradiating the gauge portion of each tensile sample in the diffractometer with the help of a specially designed holder. A schematic description of the set up is shown in figure 20. Using copper radiation and a scanning speed of 0.6° 2θ/minute, each sample was scanned nine times. The mean of the volume fraction of γ_R obtained against each of these nine readings was considered as the actual volume fraction of γ_R for any one condition.

Since the γ_R phase tends to transform to martensite at the slightest deformation, the heat treated samples after being polished mechanically up to 0.05 μ level, were polished chemically. This was done by immersing the samples in a solution consisting of a mixture 80 mℓ H_2O_2 (30%), 18 mL distilled water and 5 mL HF (52%)[131].

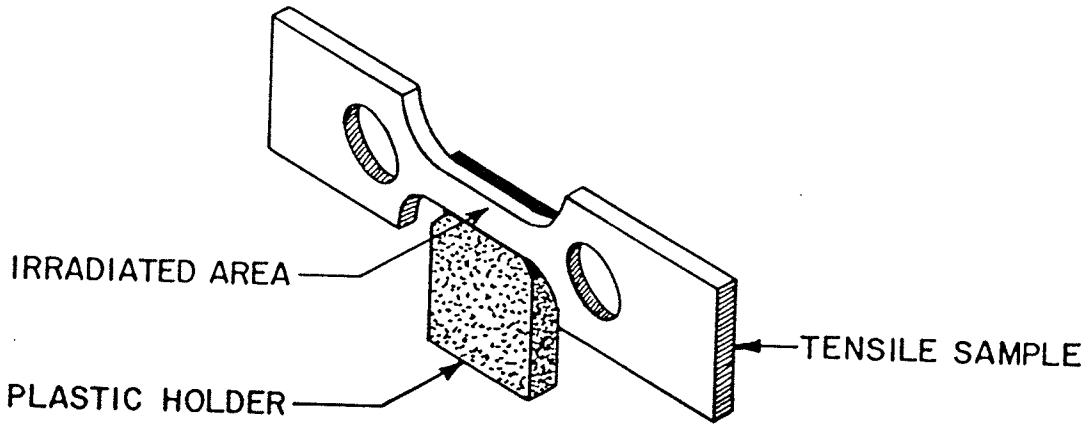

(a)

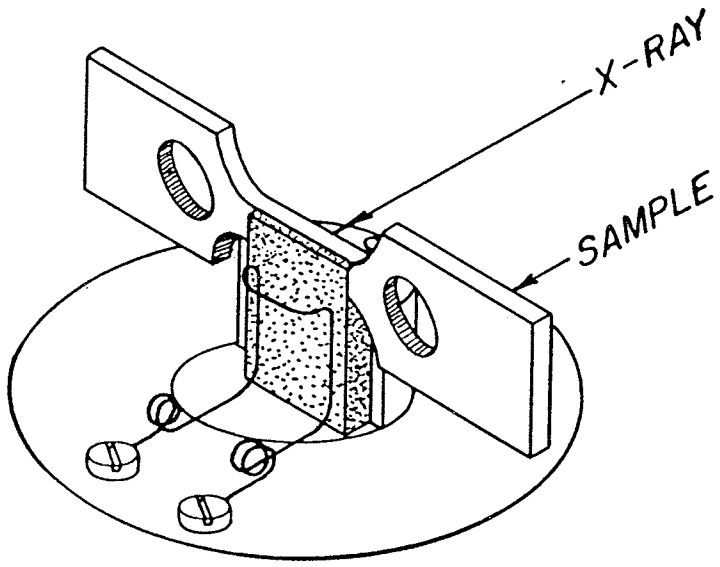

(b)

Figure 20 Schematic view of, (a) the tensile sample mounted in the specially designed plastic holder and (b) the tensile specimen with the holder in the diffractometer camera.

The equipment used for the analysis was a Philips-1710 Automatic Poneder Diffractometer unit of the Earth Science Department of the University of Manitoba.

4.6 Mechanical Tests

Limited tensile tests were carried out to determine the ease with which the γ_R phase in the samples would transform to martensite when subjected to tensile loading. The tests involved straining the samples in steps up to 1, 3 and 5% (Engg strain) in steps at a strain rate of 6×10^{-3} sec^{-1}. Between consecutive steps the γ_R volume fraction was measured.

CHAPTER V

RESULTS

5.1 Starting Microstructures

Figs. 21 to 23 show the three different starting microstructures (Q,QT and F+P) obtained as a result of the various heat treatments given to the hot rolled plates. Q starting structure (Fig. 21) consists of fine martensite laths with small amounts of pro-eutectoid ferrite. The presence of fine carbide particles within the martensite packets as well as at the lath boundaries due to the tempering of the as quenched plates is evident in the QT starting structures (Fig. 22). F+P starting structure (Fig. 23) consists of large ferrite and pearlite grains. The grains are coarse due to annealing at relatively high temperatures (940°C) and long holding time (12 hrs.).

5.2 Retention of Austenite

Austenite retention in this type of steels, as stated in section 3, is expected to be influenced by various annealing parameters such as time and temperature of annealing, cooling rates and starting microstructure. Experimental results on the effect of these variables on austenite retention are presented in the following sections.

5.2.1 Effect of Various Starting Microstructures. The effect of starting microstructure on the austenite retention for samples annealed at various temperatures followed by air cooling is shown in figure 24. It is seen that tempered martensitic (QT) starting microstructure allows the retention of more austenite for all annealing temperatures, as

x 1000

Figure 21. Micrograph of as quenched (Q) starting structure. The white patches represent pro-eutectoid ferrite [etched with 2% nital].

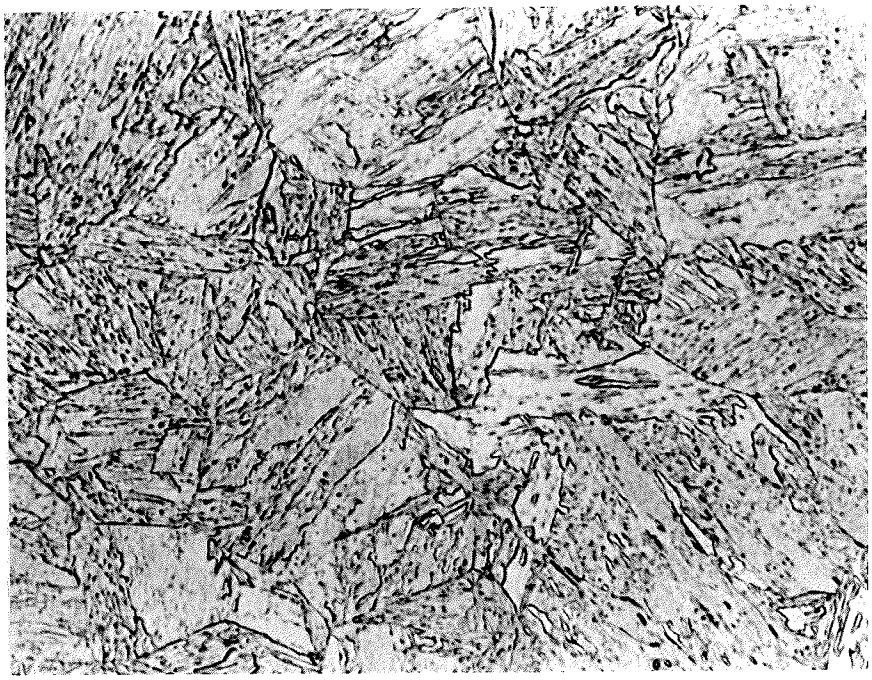

x 1000

Figure 22. Micrograph of quenched and tempered(QT) starting structure. The fine particles represent the carbide precipitated within the martensite packets at the lath boundaries as a result of the tempering treatment [etched with 2% Nital].

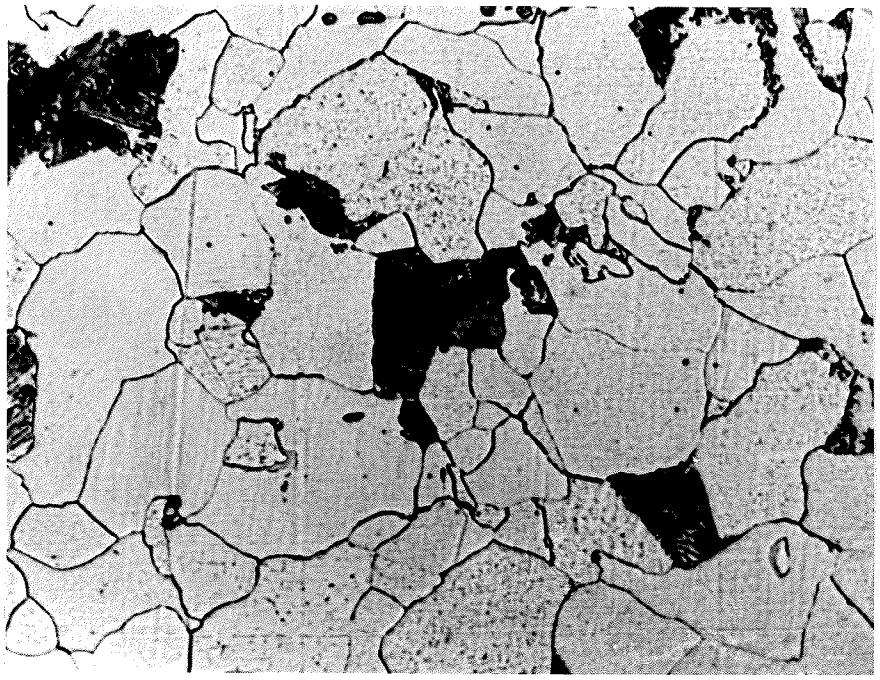

X 1000

Figure 23. Micrograph of ferrite and pearlite (F+P) starting microstructure. Pearlite (dark) grains are visible in a matrix of ferrite (grey) grains. [Etched with 2% Nital].

compared to the other two starting structures. The conventional ferrite-pearlite (F+P) starting structure yields the least amount of γ_R an annealing at any temperature within the temperature ranges studied. The martensitic (Q) starting structure allows retention of slightly higher amounts of γ_R than those obtained by using (F+P) starting structure.

Typical micrographs of air cooled samples of three different starting microstructures after annealing at 792°C for 3 minutes are shown in Figs. 25 to 27. Fig. 25 shows that most of the austenite formed during I.C. annealing of samples with F+P starting microstructure is nucleated at ferrite/ferrite and ferrite/pearlite boundaries as mentioned in section 3.2. That some austenite has also nucleated within the ferrite grains is also evident in this figure. The general morphology of the austenite particles formed with Q and QT starting

structures are quite similar as can be seen in Figs. 26 and 27. The austenite particles formed during intercritical annealing are mostly acicular in shape, although some equiaxed particles are also present in both the microstructures. A closer examination of these two figures shows that the average size of the austenite particles is larger for QT starting structure compared to that for Q starting structure.

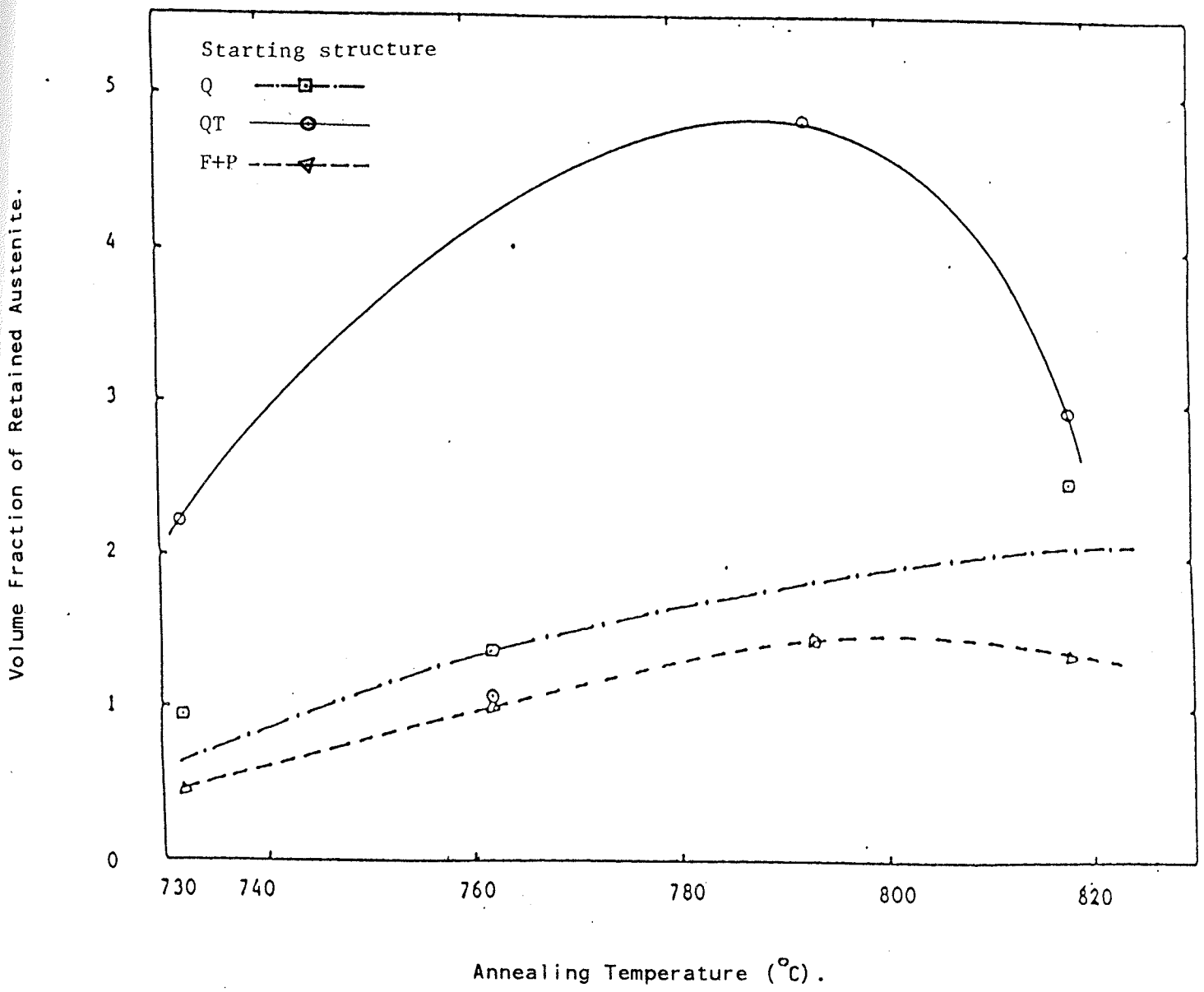

Figure 24. Volume fraction of austenite retained as a function of annealing temperature for various starting microstructures.

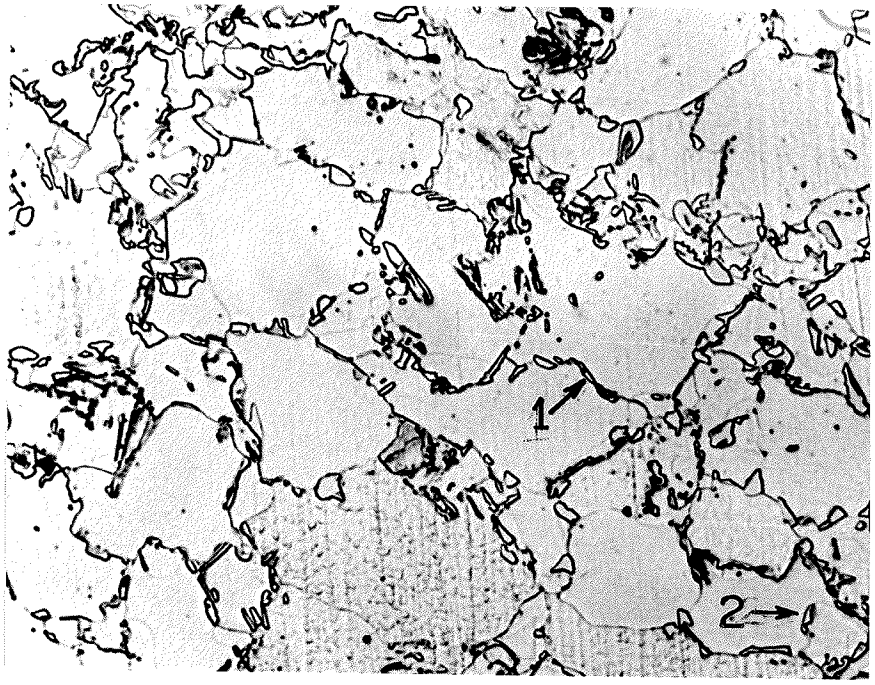

X1000

Figure 25. Micrograph of air cooled sample with (F+P) starting structure after annealing at 792°C for 3 minutes. Austenite formation at grain boundaries (marked 1) is evident. Occasional cases of austenite formation within the grains (marked 2) are also visible [2% Nital etched].

X1000

Figure 26. Micrograph of air cooled sample with Q starting structure after annealing at 792°C for 3 minutes. Austenite, retained as well as transformed are in the form of acicular and equiaxed particles in a matrix of ferrite [2% Nital etched].

5.2.2 Effect of Annealing Temperature. The plots in Fig. 24 also indicate that for F+P and QT starting structures, the volume fraction of γ_R increases with increasing annealing temperature up to 792°C. Further rise in the annealing temperature brings about a rapid decrease in the volume fraction of this phase. However in the case of Q starting microstructures, the amount of austenite retained increases continuously within the observed range of annealing temperatures.

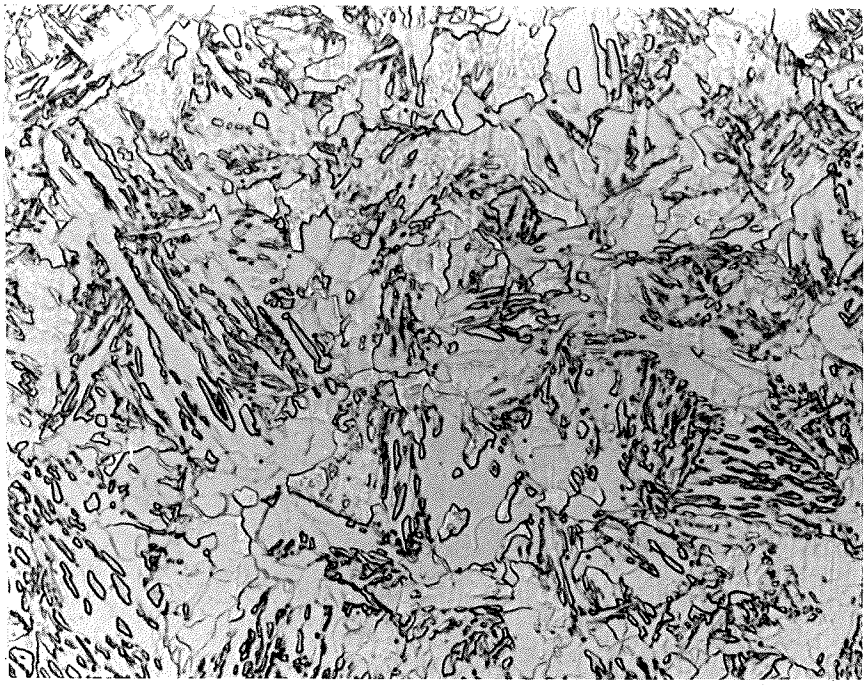

X1000

Figure 27. Micrograph of air cooled sample with QT starting structure after annealing at 792°C for 3 minutes. Austenite retained as well as transformed are in the form of acicular and equiaxed particles in a matrix of ferrite. Note that the average size of these particles is larger than those in Figure 26. [2% Nital Etched]

5.2.3 Effect of Annealing Time. As can be seen from Fig. 24, the γ_R volume fraction for samples with QT starting is higher than that with Q and F+P starting structures for all annealing temperatures. Therefore the effect of annealing time on austenite retention was investigated at various annealing temperatures using samples with this starting

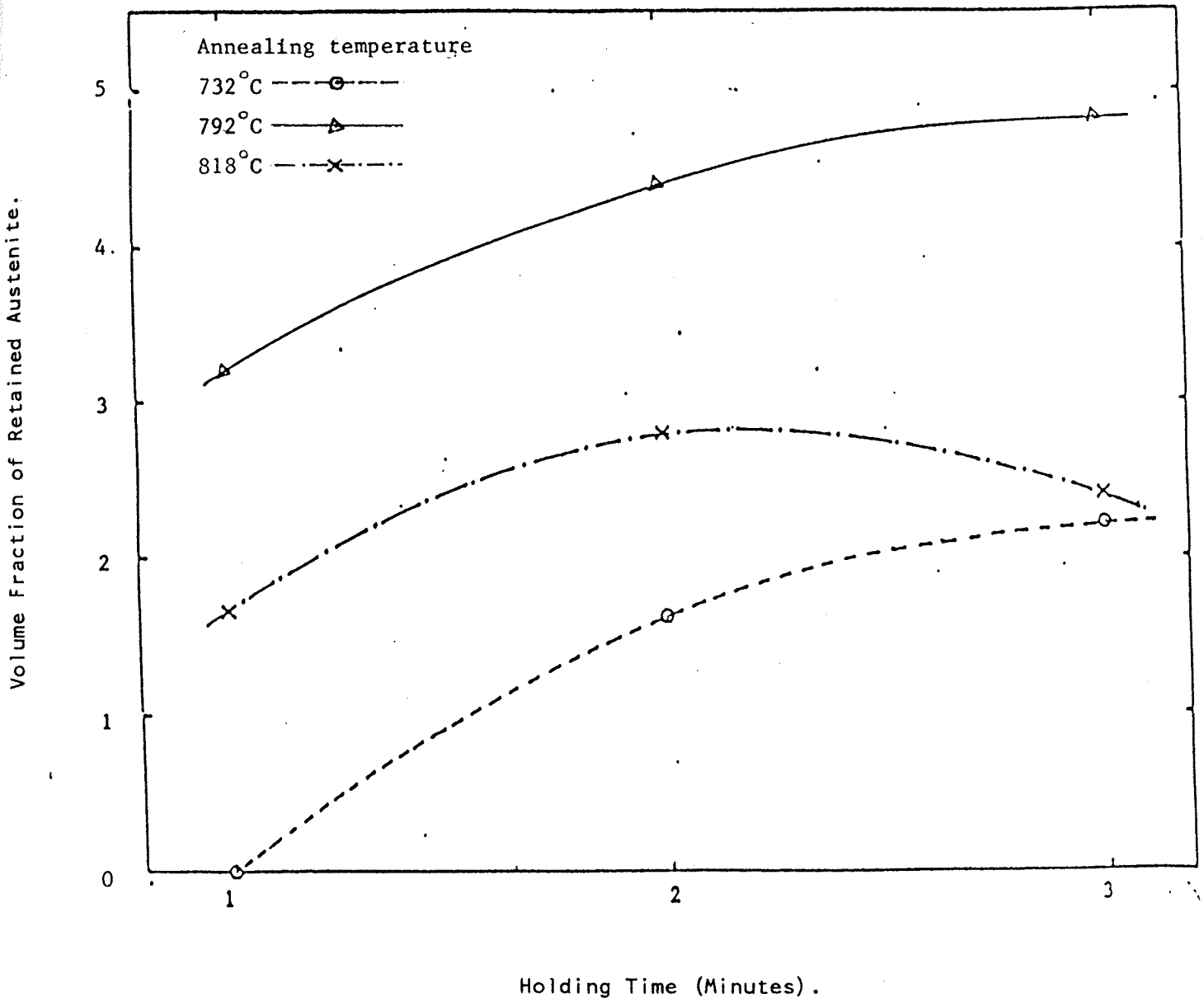

Figure 28. Volume fraction of austenite retained as a function of annealing time at different annealing temperatures for samples with QT starting microstructure.

(between 1 and 3 minutes) at 732°C, 792°C and 818°C. As can be seen from this figure, the volume fraction γ_R for the sample annealed at 818°C increases with increasing annealing time up to 2 minutes beyond which it decreases. Also the annealing time for which maximum amounts of austenite is retained appears to vary with the annealing temperature in the following manner.

2 minutes at 818°C

> 3 minutes at 792°C

>> 3 minutes at 818°C

5.2.4 Effect of Post Annealing Cooling Rates

No measurable amounts of γ_R were retained when samples with starting microstructures as shown in Figs. 21 to 23 were quenched in oil or water after intercritical annealing for 3 minutes at various annealing temperatures considered in this study. This is unlike the case of air cooled samples, results of which are shown in Fig. 24.

5.3 Stability of Retained Austenite Against Deformation Induced Martensitic Transformation

The stability of γ_R, in addition to its volume fraction, is known to have significant influence on the strength-ductility combination of dual phase steels[42]. It is therefore desirable to evaluate the stability of this phase obtained by intercritically annealing samples with different starting structures under various annealing conditions.

As has been observed during in situ straining of thin foils of intercritically annealed dual phase steel samples in TEM, the stability

of γ_R is related to its particle size[43] (the smaller the size of γ_R particles, the higher the strain required to transform it).

Since the size of γ_R particles that are retained in samples with various starting structures after intercritically annealing them under different annealing conditions is expected to be vary in size, the stability of γ_R in different samples is therefore also expected to be different. Measurement of γ_R volume fraction in these samples after straining to various strain levels may therefore provide an indirect information about the particle size of γ_R.

5.3.1 Effect of Starting Structure on the Mechanical Stability of γ_R.

Fig. 29 shows the untransformed volume fraction of γ_R (normalized to 1) as a function of applied strain for samples with all the three different starting structures which were annealed at 792°C for 3 minutes and air cooled. The following observations may be made from this figure.

1) In the sample with (F+P) starting structure, γ_R to martensite transformation started immediately after straining and the rate of transformation is so rapid that all the γ_R transforms to martensite up to 5% applied strain.

2) The rate of transformation of γ_R to martensite in the sample with QT starting structure is slower than in the sample with (F+P) starting structure.

3) In the sample with Q starting structure, initially (up to about 3% strain) there is hardly any transformation of γ_R to martensite. However, after 3% strain, γ_R starts transforming to martensite.

The above observations suggest that stability of γ_R in samples with Q and QT starting structures is much higher than that of samples with (F+P) starting structure.

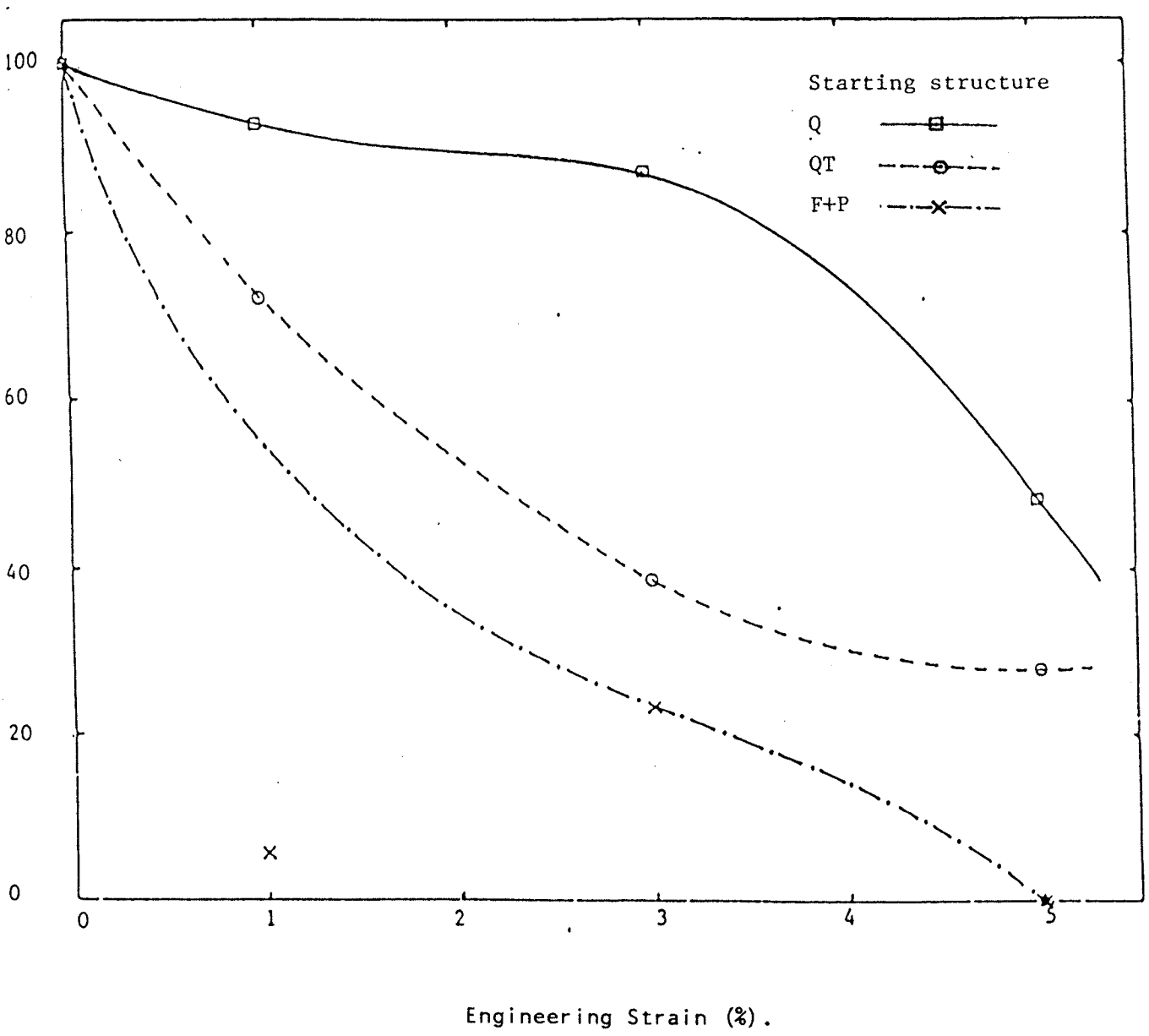

Figure 29. Volume fraction of austenite retained as a function of tensile strain in air cooled samples with various starting microstructures annealed at 792°C for the same length of time.

5.3.2 Effect of Annealing Temperature and Time on the Mechanical Stability of γ_R

In view of the fact that the samples with QT structure resulted in higher volume fraction of γ_R by annealing under different conditions, the study of the effect of annealing temperature and time on the mechanical stability of γ_R was limited to samples with QT starting structure only.

Figs. 30 and 31 show the volume fraction of untransformed (normalized to 1) γ_R as a function of applied strain for samples with QT starting structure which were annealed at different temperatures for a fixed time (Fig. 30) and annealed at a fixed temperature for varying times (Fig. 31) respectively and subsequently cooled in air. The following observations may be made from these figures:

1) The rate of transformation of γ_R to martensite in the sample which is annealed at 792°C is much faster than that in the sample which is annealed at 732°C (Fig. 30).

2) The rate of transformation of γ_R to martensite in the sample which is annealed at 792°C for 3 minutes is faster than that in the sample which is annealed at 792°C for 2 minutes.

The above observations indicate that the stability of γ_R against deformation induced martensitic transformation is increased by lowering, either the annealing temperature or annealing time while the other annealing parameters remain constant.

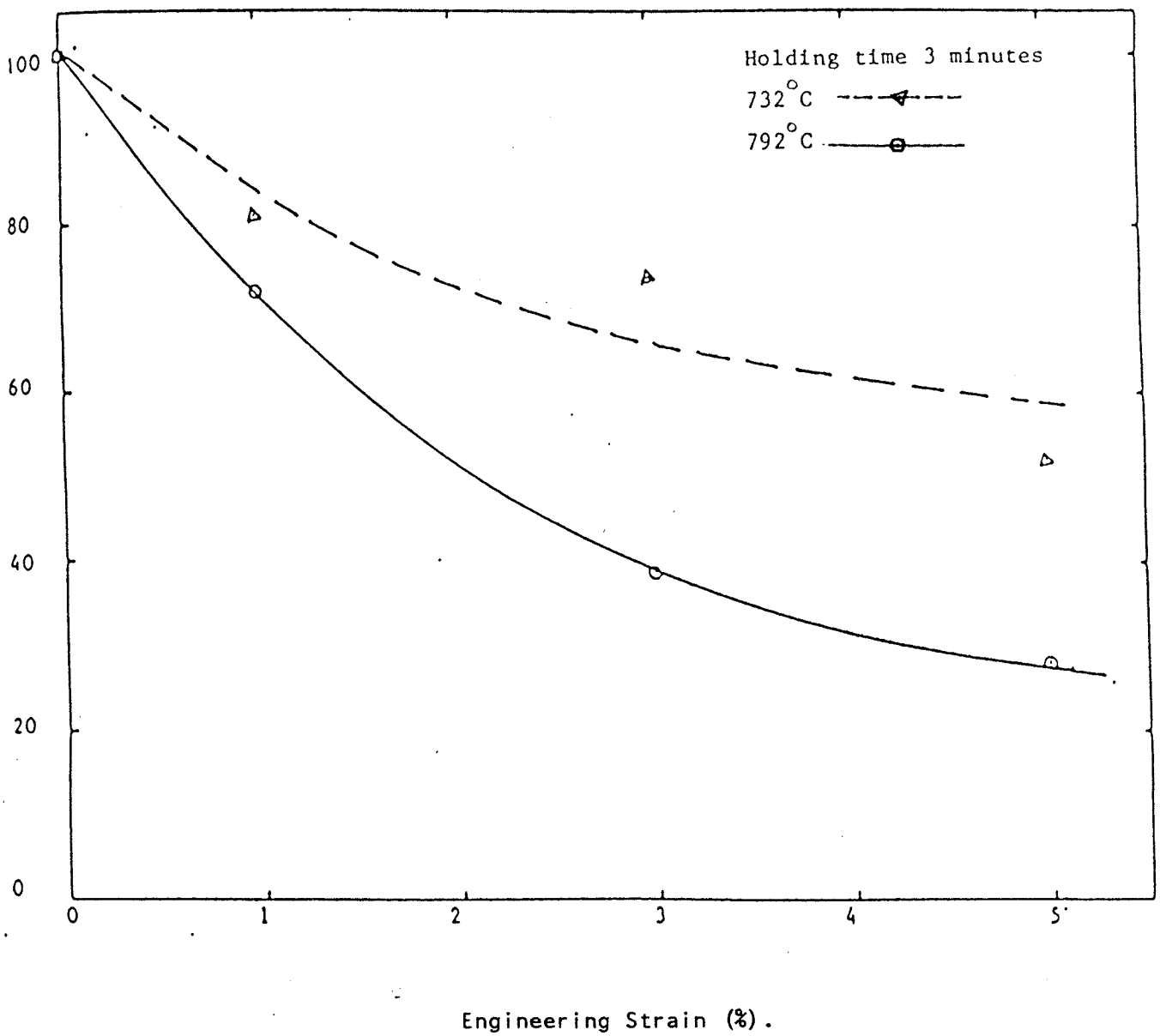

Figure 30. Volume fraction of austenite retained as a function of tensile strain in air cooled samples with QT starting microstructure annealed at two different temperatures for the same length of time.

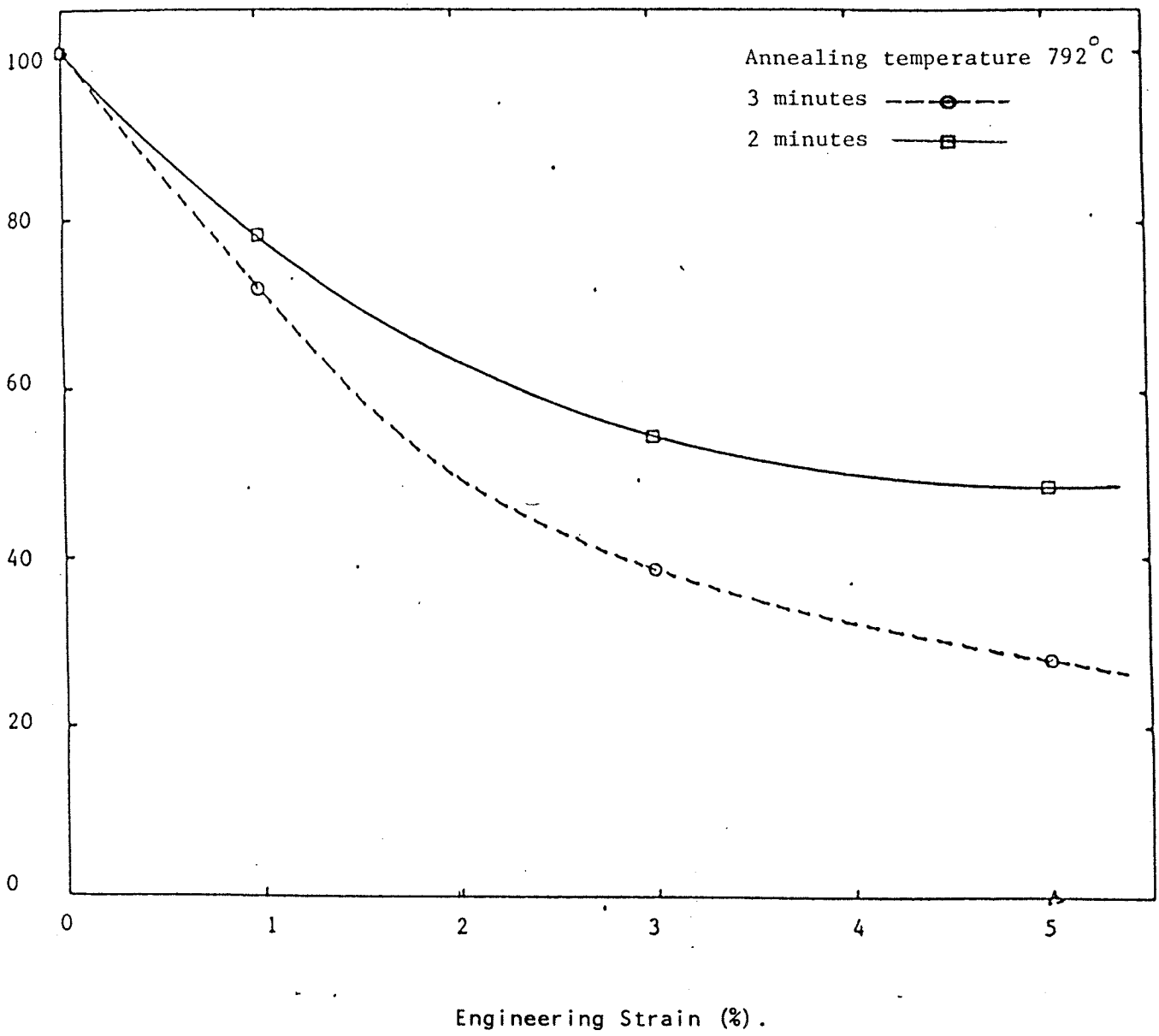

Figure 31. Volume fraction of austenite retained as a function of tensile strain in air cooled samples with QT starting microstructure annealed at identical temperature for different lengths of time.

CHAPTER VI

DISCUSSION

The results presented in the last chapter on the observed variation in the volume fraction of retained austenite as a function of starting microstructure and annealing conditions will now be explained in the light of various austenite retention mechanisms and kinetics of reaustenization as discussed earlier. It has been pointed out in Chapter 3 that isolated type of γ_R is most commonly observed in inter-critically annealed dual phase steels which are slow cooled, whereas capsulated type or some inter lath type of austenite is observed in rather rapidly cooled dual phase steels. In the present study, measurable amounts of γ_R (using x-ray diffraction techniques) were obtained only in air cooled samples. Therefore it is expected that the majority of γ_R particles in the annealed samples are of the isolated type. The stabilization mechanism of the isolated type of γ_R has been attributed mainly to the size stabilization effect. The austenite particles which may have grown during annealing at intertricritical temperatures undergo some shrinkage during cooling. The extent of austenite shrinkage increases with decreasing cooling rates. With a decrease in the cooling rate, the reduction in the size of austenite particles is brought above by the movement of the ferrite/austenite interface over relatively larger distances caused by the formation of higher volumes of proeutectoid ferrite, leaving isolated austenite particles (at temperatures just M_s) which are prone to retention. Size stabilization effect provides an important rationale to explain the

results of variation in γ_R volume fraction with starting microstructure and annealing conditions as discussed in the following sections.

6.1 Effect of Various Starting Microstructures

The differences in the amounts of austenite retained in samples with different starting structures (Q,QT and F+P) after annealing at various temperatures in the two phase regimes ($\alpha + \gamma$ region) of the Fe-C equilibrium diagram are mainly due to the presence of different kinds of interfaces present in these structures. These interfaces effect the nucleation and growth of austenite during intercritical annealing in different manners for steels with different starting structures. As mentioned earlier (Chapter 3), the martensite lath boundaries (MLB) have a significant influence in restricting the growth of austenite particles that are nucleated at the carbide/MLB interface during annealing. Therefore, it is expected that the austenite formed in samples with starting structures containing MLB (for example in samples with Q and QT structures) is more prone to retention than in samples without MLB (such as samples with F+P structures). As shown in Fig. 24 (Chapter 5), the volume fraction of γ_R is highest in samples with QT starting structure and lowest for samples with F+P starting structure. For samples with Q starting structure, the volume of γ_R is intermediate between those of QT and F+P starting structures. The fact that MLB does restrict the growth of nucleated austenite in Q and QT structures making it more prone to retention during cooling compared to that in F+P structure, as observed from Fig. 24, can be further supported by considering the following argument.

The austenite nucleation rate ($\dot{N}$) can be considered to be proportional to the density of the potential nucleation sites ($\frac{S}{A}$) where S is the total number of readily available carbide particles present in a given volume of the steel. A is the total interfacial area (giving rise to triple junctions) within the same volume of the steel

Thus the nucleation rate for the two different starting micro structures can be written as

$$\dot{N}_{F+P} \propto \frac{S_{F+P}}{A_{F+P}} \quad \text{(for F+P starting structure)}$$

and

$$\dot{N}_{Q} \propto \frac{S_{Q}}{A_{Q}} \quad \text{(for Q starting structure)}$$

Here $A_Q >> A_{F+P}$, because each martensite lath in the Q starting structure is considerably smaller than any of the ferrite or pearlite grains in the F+P starting structure as can be seen from Figs. 21 and 23. Also $S_Q << S_{F+P}$, because the F+P starting structure was obtained by a slow cooling process enabling a significantly larger number of carbides to precipitate, unlike the case of Q starting structure which was obtained by rapid cooling from the austenitizing temperatures. Therefore, the austenite nucleation rate in (F+P) starting structure will be higher than in Q starting structure (i.e., $N_{F+P} > \dot{N}_Q$).

If the growth kinetics of the nucleated austenite for the two different starting structures are identical, the average size of the austenite particles formed with F+P starting structure will be smaller than those obtained from Q starting structure. Under such conditions,

it is expected that F+P starting microstructure will permit retention of more austenite as compared to the Q starting structure. However, the observations made from Fig. 24 indicate the opposite (i.e., the volume fraction γ_R for samples with Q structure is higher than that for F+P structure).

This can happen only if

$$\dot{G}_{F+P} >> \dot{G}_Q$$

where $\dot{G}_{F+P}$ and $\dot{G}_Q$ on the growth rates of austenite in samples with F+P and Q starting structures, respectively.

$\dot{G}_{F+P}$ in fact is expected to be higher than $\dot{G}_Q$ since there are no martensite lath boundaries present in the F+P starting structure which may inhibit the growth of austenite nucleated in sample with this starting structure.

Also it is observed in Fig. 29, that the stability of the γ_R phase, is superior in samples with Q starting structures than in samples with F+P starting structures. As it is quite well established that the stability of γ_R against disformation induced transformation to martensite is enhanced with the decrease in the particle size of this phase, the results of this test therefore corroborate the conclusion that austenite growth rate in samples with F+P starting structure is higher than that in samples with Q starting structure.

Higher amounts of γ_R obtained in samples with QT starting structure compared to that obtained in samples wtih Q starting structure can be explained as follows: Specimens with Q starting structure, when heated to the desired annealing temperature, undergo a very rapid tempering process during which carbide particles precipitate at the martensite lath boundaries[128]. This structure then becomes similar to the QT

structure and on heating the austenite is nucleated at the triple junctions of these carbides and martensite lath boundaries as explained in Chapter 3. This step, although rapid, consumes a part of the annealing time. Thus the effective holding time for samples with Q starting structure is smaller than that for samples with QT starting structure despite the fact that samples with both these starting structures were annealed for the same length of time (3 minutes). The shorter holding time (effective) therefore results in the formation of smaller amounts of austenite in samples with Q starting structure which in turn allows the retention of smaller amounts of γ_R as compared to QT starting structure. The differences in the retention behaviour of austenite for samples with Q and QT structures reflect the significance of annealing time as a controlling parameter during intercritical annealing of dual phase steels. This aspect will be further discussed in a later section.

In conclusion, it may be stated that in order to retain higher volume fractions of austenite, it is desirable to have a starting structure which has a high density of potential austenite nucleation sites in conjunction with a large number of structural barriers like martensite lath boundaries to inhibit the growth of austenite nucleated during annealing.

6.2 Effect of Annealing Temperature

As seen from Fig. 29 (Chapter 5), the general trend of the profiles of γ_R versus annealing temperature curves was very similar for F+P and QT structures. For samples with both these starting structures, the γ_R volume fraction increased with increasing annealing temperature up to

792°C. The amount of γ_R decreased by annealing beyond this temperature. For samples with Q starting structure, the γ_R volume fraction increased with increasing annealing temperature in the range of temperatures studied in this work. As mentioned earlier, the formation of austenite during the intercritical annealing of steels is a nucleation and growth process that is influenced by the starting structure. For samples with QT and F+P structure, more and more austenite particles nucleate with increasing temperature up to 792°C (for a constant annealing time of 3 mins.) without undergoing any significant growth as schematically shown in Fig. 32 (a to c) for temperatures up to T_3. These nucleated austenite particles, being very small, are prone to retention during cooling and as such are retained in increasing amounts with increasing temperatures whereas those austenite particles which may have grown are transformed. However, at temperatures above 792°C once the austenite particle is nucleated, significant growth of the particle takes place. As a result, by annealing above 792°C the bulk of the total austenite volume at the end of 3 minutes holding time consists of particles that have undergone significant growth Figs. 32 (d to f). Therefore, although the total volume of austenite formed increases with increasing temperature, the amount of austenite retained decreases since the number of smaller austenite particles that are prone to retention decreases. Thus it appears that the kinetics of austenite formation during reaustenization in samples with QT and (F+P) starting structure is mainly controlled by nucleation of austenite between A_1 temperature and 792°C and by growth of austenite between 792°C and A_3 temperature. For Q starting structure, however, it appears that the kinetics are mainly governed by the nucleation of austenite within the range of temperatures studied in this work.

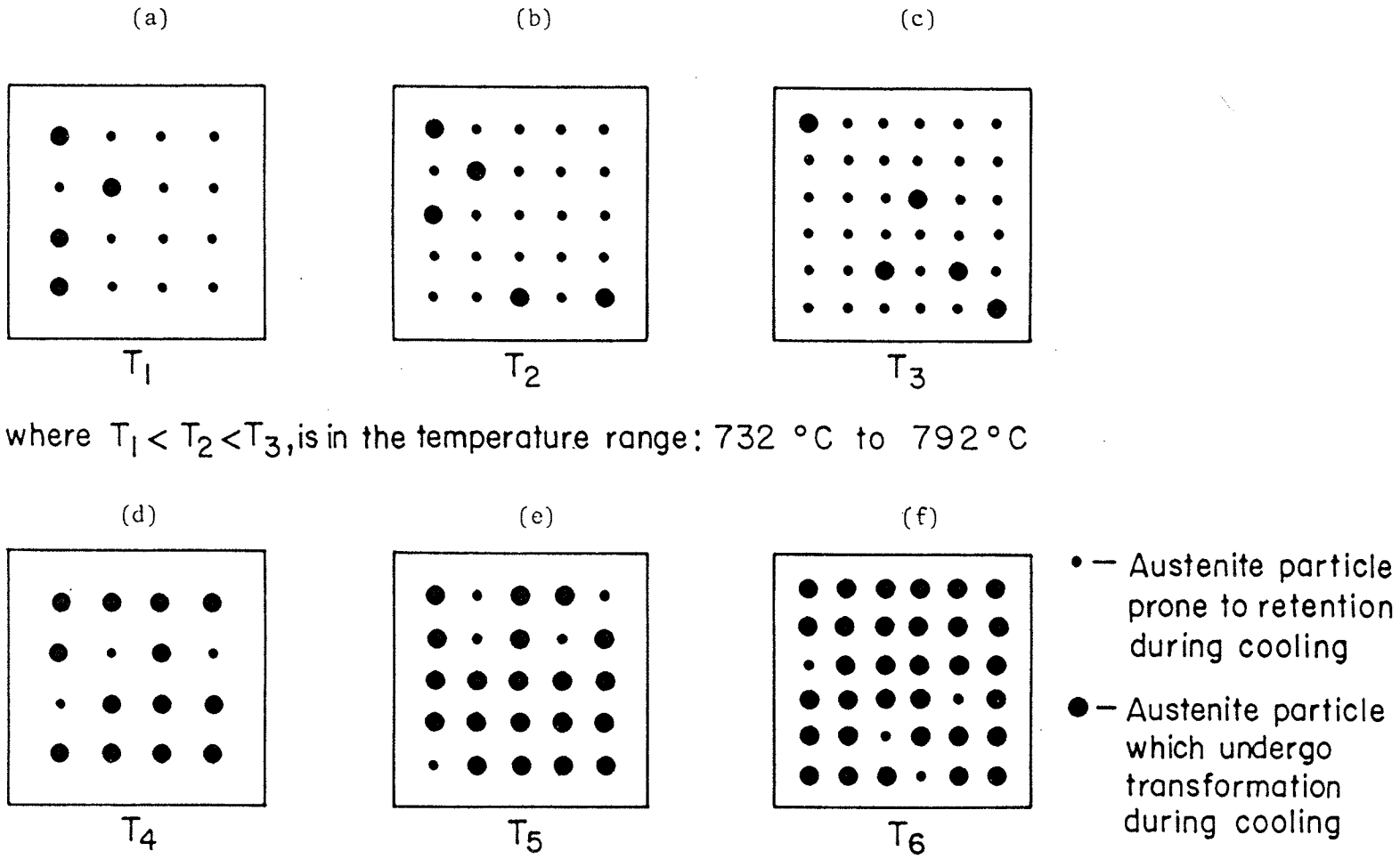

Figure 32. Schematic diagram showing nucleation kinetics dominated (a to c) and growth kinetics dominated (d to f) austenite formation during intercritical annealing

To verify the rationale presented above, samples with QT starting structures which were annealed for 3 minutes at 732°C and 792°C were strained to various strain levels to determine the stability of γ_R in the respective samples against deformation induced transformation. Figs. 27 and 33 represent the microstructure of samples subjected to these two annealing treatments. It is observed from these micrographs that the average size of the second phase particles is smaller in the sample annealed at 732°C. This suggests that the γ_R particles retained

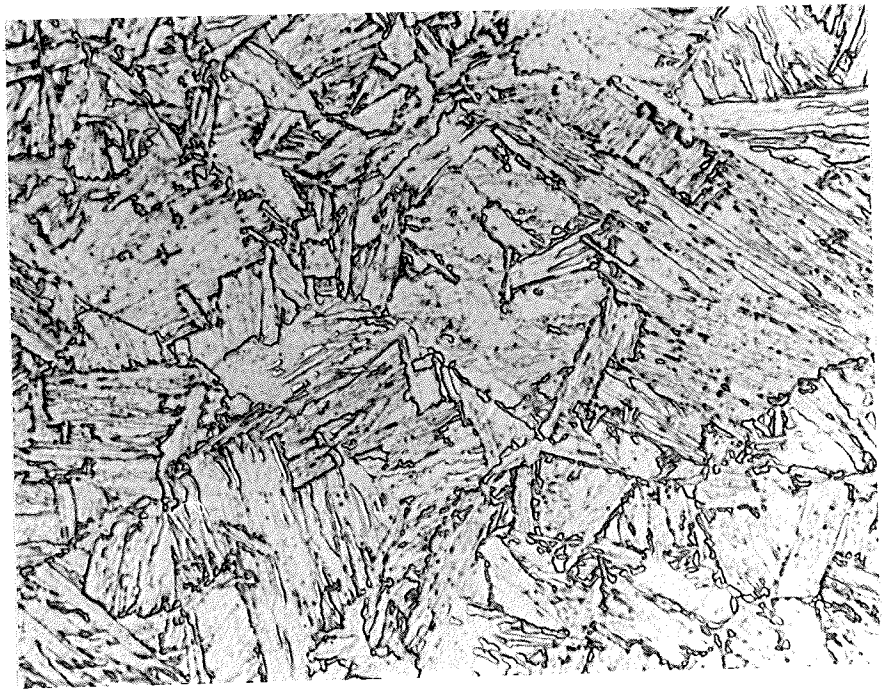

Figure 33. Micrograph of air cooled sample with QT starting structure annealed at 792°C for 3 minutes. Austenite retained as well as transformed are in the form of acicular and equiaxed particles in a matrix of ferrite. Note that these particles are significantly finer than those in Figure 30.

an annealing at 732°C is finer than those retained after annealing 792°C. As shown in Fig. 30, γ_R obtained after annealing at 792°C transformed with relative ease as compared to that obtained after annealing at 732°C. Since the annealing time used is rather short (3 minutes), the variation in the chemistry of the austenite formed at these two temperatures is not expected to be significant. It also suggests that the mean size of the austenite particles retained on cooling from the higher temperature is larger as compared to those retained after annealing at 732°C. The results in Figs. 24 and 30 indicate that despite the increase in the average size of the austenite particles as the annealing temperature is raised up to 792°C, there is an increase in the volume of austenite that is retained. This corroborates the suggestion that between A_1 temperature and 792°C the austenite nucleation kinetics has an overriding influence over its growth kinetics during the process of austenite formation. Therefore the change in the trend of austenite retention with the rise in the annealing temperatures beyond 792°C represents a reversal in the basic characteristics of austenite formation that prevail between A_1 temperatures and 792°C.

6.3 Effect of Annealing Time

The effect of annealing time on the retention of austenite as stated in section 5.2.4 was studied on samples with QT starting structures. Fig. 28 shows that for any annealing temperature, there is an increase in the amount of austenite retained withincrease in the annealing time up to a certain level. Beyond this time, there is a gradual decrease in the volume of austenite retained with the increase

in time. This trend is also indicative of the fact that austenite formation as a function of holding time is dominated by the austenite nucleation kinetics up to a certain time limit. The domination of the nucleation kinetics gradually diminishes with increasing time giving rise to a situation in which the growth kinetics starts dominating the reaction process. In other words the effect of annealing time, on austenite retention is analogous to that of annealing temperature.

Fig. 31 indicates that the average size of the γ_R particles obtained after annealing for 2 minutes is finer than those obtained after annealing for 3 minutes. Despite the coarsening of the austenite particles that are formed during annealing with increasing holding time, there is an increase in the amount of austenite that is retained (Fig. 28). These observations suggest that the conclusions made earlier about the existence of an initial time regime in which the effect of nucleation kinetics overrides that of growth kinetics, is correct.

Another noticeable feature in Fig. 28 is that the time for the maximum austenite retention increases with decrease in the annealing temperature. This can be attributed to the consumption of the possible nucleation sites over shorter time intervals and consequently an increasingly early onset of the growth process, as the annealing temperature is raised.

Thus it is concluded that for tempered martensitic starting structure there exists a critical combination of annealing time and temperature corresponding to which maximum austenite can be retained in this steel.

CHAPTER VII

CONCLUSIONS

For the steel studied the following conclusions can be drawn from the results.

i) The process of austenite formation during intercritical annealing is controlled by the austenite nucleation kinetics up to a certain temperature. Above this temperature, the reaction is controlled by the growth kinetics of austenite. This is true for starting microstructures consisting of ferrite + pearlite, and tempered martensite.

ii) For the tempered martensite starting microstructure, austenite formation at any intercritical annealing temperature is dominated by the nucleation kinetics up to a certain time. At greater times the growth kinetics dominate the reaction.

iii) Compared to the conventional ferrite + pearlite starting microstructure, the quenched and tempered starting microstructure results in the retention of significantly larger amounts of γ_R for a given set of annealing conditions.

iv) The austenite retained on intercritical annealing of samples with tempered martensitic starting structure has superior stability against deformation induced transformation as compared to that obtained by incritical annealing of samples with conventional ferrite and pearlite starting structure.

REFERENCES

1. M.S. Rashid, Annual Review Material Sec II, (1981), p. 245.

2. G.R. Speich, Fundamentals of Dual Phase Steels, Kot and Bramfitt (ed.), TMS-AIME pub, p. 3.

3. S. Hayami, and T. Furukawa, Microalloying 75, p. 311, Proc. Conference, Washington, D.C., New York, Union Carbide, Corp.

4. M.S. Rashid, S.A.E. Preprint 760206, Feb. (1976).

5. M.S. Rashid, S.A.E. Preprint 770211, Feb. (1977).

6. D.S. Dabkowski and G.R. Speich, Proc. Conf. Pittsburg PA, Jan 26-27 (1977), p. 284.

7. D.J. Baily and R. Stevenson, General Motors Technical Centre report G.M.R.-2373, April (1977).

8. K. Arakai, S. Fukunaka and K. Uchida, Trans ISIJ, 17 (1977), p. 701.

9. R.G. Davies, Met Trans 9A (1978) p. 41.

10. R.G. Davies, Met Trans 9A (1978) p. 671.

11. K. Arakai, Y. Takada and K. Nakoaka, Trans ISIJ, 17 (1977), p. 710.

12. G.R. Speich and R.L. Miller, Structure and Properties of Dual Phase Steels, Kot and Morris (ed.), T.M.S.-AIME pub, p. 145.

13. I. Tamura, Y. Tomata, A. Akao, Y. Yamada, M. Ozawa and S. Kanotoni, Trans ISIJ, 13 (1973) p. 283.

14. K. Nakaoka, K. Aaraki and K. Kurihara, Formable HSLA and Dual-Phase Steels, Davenport (ed.), p. 128.

15. J. Becker and E. Hornbogen, Structure and Properties of Dual Phase Steels, Kot and Morris (eds.), TMS-AIME pub, p. 20.

16. M.S. Rashid, Formable HSLA and Dual Phase Steels, Davenport (ed.) TMS-AIME pub, p. 1.

17. P.E. Repas "Metallurgy, Production, Technology, and Properties of Dual Phase Steels" in Dual Phase and Cold-Forming Variation Steels in the Automobile Industry, Vanitec, Berlin, 1978, p. 13.

18. G. Thomas and J.Y. Koo, Structure and Properties of Dual Phase Steels, Kot and Morris (eds.), TMS-AIME pub, p. 183.

19. R.G. Davies, Met Trans 10A (1979), p. 113.

20. S. Hayami, T. Furukawa, H. Gondoh and H. Takechi, Formable HSLA and Dual Phase Steels, Davenport (ed.), p. 169.

21. A.R. Marder, Farmable HSLA and Dual Phase Steels, Davenport (ed.) TMS-AIME pub, p. 87.

22. J. Rigsbee and P.J. VanderArend, Formable HSLA and Dual Phase Steels, Davenport (ed.), TMS-AIME pub, p. 58.

23. M.S.Rashid and B.V.N. Rao, Fundamentals of Dual Phase Steels, Kot and Bramfitt (eds.), TMS-AIME pub, p. 249.

24. T. Furukawa, H. Morikawa, H. Takechi and K. Koyama, Structure and Properties of Dual Phase Steels, Kot and Morris (eds.), TMS-AIME pub, p. 281.

25. J. Y. Koo and G. Thomas, Material Science and Engrg 24 (1976), p. 187.

26. A. Okamato and M. Takahashi, Fundamentals of Dual Phase Steels, Kot and Bramfitt (eds.), TMS-AIME pub, p. 427.

27. V. Bangaru and A.K. Sachdev, Met Trans, 13A, (1982), p. 1894.

28. G.T. Eldis, Structure and Properties of Dual Phase Steels, Kot and Morris (eds.) TMS-AIME pub, p. 202.

29. G. Tither and M. Levite, J. of Metals 27 (1975), p. 15.

30. G.R. Speich and R.L. Miller, Structure and Properties of Dual Phase Steels, Kot and Morris (eds.), TMS-AIME, pub, p. 145.

31. V.F. Zackay, E.R. Parker, E.R. Fahr, D. Bush, Trans. ASM, 60 (1967), p. 252.

32. J. Hall, V.F. Zackay and E.R. Parker, Trans ASM, 62 (1969), p. 965.

33. J. P. Bressanelli and A. Moskowitz, Trans ASM, 59 (1966), p. 223.

34. F.B. Pickering, International Metals Review, Review 211 (1966), p. 227.

35. J.J. Yi, K.J. Yu, I.S. Kim and S.J. Kim, Met Trans 14A (1983), p. 1497.

36. K.R. Kinsman, G. Das and R.F. Hehemann, Acta Met 25 (1977), p. 359.

37. P.R. Mould, Metals Engr Quarterly 15 (1975), p. 22.

38. M. Niikura, M. Yamada, J. Tanaka and H. Ichinose, Proc. Int. Conf. on New Aspects of Martensitic Transformation, Kobe, Japan, (1976), p. 321.

39. Y. Bergstrom, Mat. Sci. Eng. 5 (1969), p. 193.

40. R. Vetter, A.R. Wachters and P.Jangenburger, Scr Met. 11 (1977), p. 405.

41. G.E. Dieter, Mechanical Metallurgy (2nd Edition), McGraw-Hill Book Co., N.Y. (1976), p. 342.

42. S. Sangal, M.Sc. Thesis, University of Manitoba (1985).

43. B.V.N. Rao and M.S.Rashid, Metallography 16 (1983), p. 19.

44. T. Maki, Y. Tomato and I. Tumura, J. Jpn. Inst. Met. 38 (1974), p. 871.

45. K. Nohara, Y. Ono, and N. Ohashi, J. ISI. Jpn. 63 (1977), p. 772.

46. W.J. Harris and M. Cohen, Trans AIME, 180 (1949), p. 447.

47. B. Edmondson, Acta Met, 5 (1957), p. 208.

48. S.G. Glover, JISI 200 (1962), p. 102.

49. K.R. Kinsman and J.C. Shyne, Acta Met 15 (1967), p. 1527.

50. J. Woodila, P.G. Winchell and M. Cohen, Trans AIME 215 (1959), p. 215.

51. R.B.G. Yeo, Trans AIME, 224 (1962), p. 1222.

52. E.R. Morgan and T. Ko, Acta Met 27 (1979), p. 1907.

53. G.B. Olson and M. Cohen, Acta Met 27 (1979), p. 1907.

54. M. Cohen and C.M. Wayman "Treatise in Metallurgy", J.K. Tien and J.F. Elliot (eds.), TMS-ASM, pub. (1981).

55. J.W. Christian, "Physical Properties of Martensite and Bainite" special report #93, ISI, pub. (1965), p. 1.

56. A.W. Reynolds, J. of App. Phys. 20 (1949), p. 896.

57. B. Edmondson and T. Ko, Acta Met 2 (1954), p. 235.

58. J. Philbert and C. Crussard, C.R. Acad Sci, Paris 240 (1955), p. 190.

59. F.J. Schoen and W.S. Owen, Met Trans 2 (1971), p. 2431.

60. A.H. Cottrell and B.A. Bilby, Proc Phys Society LXII (1948), p. 49.

61. M. Sarikaya, G. Thomas and J. W. Steeds, Proc. of Int. Conf. on "Advances in the Physical Metallurgy and Application of Steels", TMS pub., (1981).

62. E.P. Klier and A.R. Traiano, Trans AIME, 162 (1966), p. 1063.

63. J.W. Christian, Met Trans 13A, (1982), p. 509.

64. M. Sarikaya, Ph.D. Thesis (1982), Univ. of Calif. Berkely.

65. K.R. Kinsman and J.C. Shyne, Acta Met 14, (1966), p. 1063.

66. J.R. Patel and M. Cohen, Acta Met 1, (1953), p. 530.

67. J.M. Moyer and Y.S. Ansell, Met Trans 6A (1975), p. 1785.

68. P.M. Kelly and J. Nutting, JISI 197 (1961), p. 199.

69. H.E. McGannon (ed.), "The Making, Shaping and Treating of Steels" 9th Edition (1971), p. 1101.

70. Z. Nishyama, "Martenitic Transformation", Academic Press, N.Y. (1978).

71. H.C. Fielder, B.L. Averbach and M. Cohen, Trans ASM, 47, (1952), p. 267.

72. S.A. Kulin,M. Cohen and B.L. Averbach, Trans. AIME, 4 (1952), p. 661.

73. W.J. Harris and M. Cohen, Trans AIME, 180, (1949), p. 447.

74. C. Zener, Trans AIME, 167 (1946), p. 513.

75. L.S. Darken, Trans AIME (1946), p. 468.

76. J.C. Fisher, J.H. Holloman and D. Turnbull, Trans AIME 185 (1949), p. 691.

77. L. Kaufman and M. Cohen, Trans AIME 206 (1956), p. 1393.

78. M. Cohen, E.S. Machlin and V.G. Paranjpe, "Thermodynamics in Physical Metallurgy", ASM (1949), p. 242.

79. R.J. Weiss and K.J. Tauer, Phys. Rev 102 (1956), p. 1490.

80. H. Sato J. Jpn Inst Met 17 (1953), p. 601.

81 Y. Imai, M.I. Izumiyama and M. Tsuchiya, Sci. Rep. RITU 17 (1965), p. 173.

82. M. Izumiyama, M. Tsuchiya and Y. Imai, J. Jpn Inst Met 34 (1970), p. 291.

83. R. Kumar and A.G. Quarrell JISI, 187 (1957), p. 195.

84. K.J.L. Iyer, Scr. Met., 6 (1972), p. 721.

85. W. Steven and A.G. Haynes, JISI 183 (1956), p. 349.

86. R.B.G. Yeo, Trans AIME 227 (1963), p. 884.

87. K. Ishida and T. Nishizawa, J. Jpn Inst of Met 36 (1972), p. 270.

88. L.A. Carapella, Met Prog 46 (1944), p. 108.

89. H. Schumann and H.J. von Firks, Arch, Eisenhutt 40 (1969), p. 561.

90. G.H. Eichelman and F.C. Hull, Trans ASM, 45 (1953), p. 77.

91. I.N. Bogachev, V.F. Yegalayev and G. Ye, Zuigintseva, Fiz. Met. Metalloved, 28 (1969), p. 885.

92. W.J. Barret and A.R. Troiano, Trans AIME, 175 (1948), p. 910.

93. M.R. Meyerson and S.J. Rosenberg, J. Res Nat Bur Std 55 (1955), p. 177.

94. W.C. Leslie and R.L. Miller, Trans ASM, 57 (1964), p. 972.

95. M. Izumiyama, Sci Rep. IRTU, (Tohoku Univ), 14 (1962), p. 11.

96. G. Krauss Jr and M. Cohen, Trans AIME, 224 (1962), p. 1212.

97. G. Krauss Jr and M. Cohen, Trans AIME, 227 (1963), p. 278.

98. Z. Nishiyama, J. Jpn Int Met., 23 (1938), p. 202.

99. O.P. Maximova and V.V. Nemirovsky, Dakl, Acad Nauk SSSR 177, No. 1 (1967), p. 81.

100. R.E. Hummel, J.W. Koger and W. Pasupathi, Trans AIME 241 (1968), p. 249.

101. R.E. Cech and D. Turnbull, Trans AIME, 206 (1956), p. 124.

102. S. Nagashima and Z. Nishiyama, J. Jpn Inst Met, 23, (1959), p. 728.

103. Y. Kachi, Y. Bando and S. Higuchi, Jpn J. Appl Phys, 1, (1962), p. 307.

104. Y. Bando, Trans JIM, 5, (1964), p. 135.

105. Y.A. Klyachko and Y.J. Baranova, Fiz Met Metalloved, 25, (1968), p. 569.

106. R.C. Bowe, L. Muldaver and F. Chambers, Scr Met, 4 (1970), p. 581.

107. V. Raghavan and A.R. Entwisle, Special Report #93, 181 (1965), p. 30.

108. V. Raghavan, Acta Met, 17, (1969), p. 1299.

109. S.R. Pati and M. Cohen, Acta Met, 17, (1969), p. 189.

110. C.H. Shih, B.L. Averbach and M. Cohen, Trans AIME, 203 (1955), p 183.

111. R.L. Fullman, Trans AIME, 197 (1953), p. 447.

112. J.C. Fisher, Trans AIME, 197 (1953), p. 918.

113. H. Knapp and U. Dehlinger, Acta Met, 4 (1956), p. 289.

114. Y. Imai and M. Izumiyama, J. Jpn Inst. Met 27 (1963), p. 171.

115. A.R. Entwisle, Met Trans, 2 (1971), p. 2395.

116. U.R. lenel and R.W.K. Honeycomb, Proc. of Int. Conf. on "Advances in the Physical Metallurgy and Applications of Steels", TMS Pub. (1981), p. 38.

117. N.C. Law and D.V. Edmonds, Met Trans A, 11A (1980), p. 33.

118. N,K. Balliger and T. Glodman, Met Sci, 15 (1981), p. 95.

119. V. Biss and R.L. Cryderman, Met Trans, 2 (1971), p. 2267.

120. J.M. Rigsbee, Proc. ICOMAT-79, W. Own (ed.), MIT Press, Cambridge, MA (1979), p. 381.

121. D.K. Matlock, G. Krauss, L.F. Ramos and G.S. Huppi, Structure and Properties of Dual Phase Steels, Kot and Morris (eds.), TMS-AIME pub, p. 62.

122. A. Hultgren, Tran ASM, 39 (1947), p. 915.

123. G.A. Roberts and R.F. Mehl, "The Mechanism and Rate of Formation of Austenite from Ferrite-Cementite Aggregate", Trans ASM, 31 (1943), p. 613.

124. R.R. Judd and H.W. Paxton, Trans AIME, 242 (1968), p. 206.

125. D.A. Porter and K.E. Easterling, "Phase Transformation in Metals and Alloys", Van Nostrand Reinhold Co., 1981.

126. S.W. Thompson, G.S. Fan and P.R. Howell, to be published in "Phase Transformations in Ferrous Alloys", Marder (ed.), TMS-AIME pub.

127. M.R. Plichita and H.I. Aarenson, Met Trans 5 (1974), p. 2611.

128. S. Watanabe, Y. Ohmori, and Tatsuro Kunitake, Proc. Int. Conf. on New Aspects of Martensitic Transformation, Kobe, Japan (1976), p. 369.

129. C.F. Jatczek, J.A. Larson and S.W. Shin, "Retained Austenite and its Measurements by X-Ray Diffraction", Rept. No. 453 (1980), pub SAE Inc. 400 Commonwealth Drive, Warrendel, PA.

130. B.W. Christ and L.C. Smith, JISI, 211 (1973), p. 155.

131. S.Watanabe, Y. Ohmari and T. Kunitake, Proc. of Jpn. Inst. Met. Ints. Symp. on New Aspects of Martensitic Transfn, p. 369.

132. K.W. Andrew, JISI, 203 (1965), p. 721.

133. G.R. Speich, V.A. Demerest and R.L. Miller, Met Trans, 12A (1981), p. 1419.

134. B.D. Cullity, "Elements of x-ray diffraction", pub. Addison-Weseley, Reading, Massachusetts, 1956.

135. R.W. James, "The Optical Principles of the Diffraction of X-rays", Appendix III, pub. G. Bell and Sons, London (1967).

APPENDIX I

1. Contributions of Chemical and Austenite Particle Size Stabilization Effects in Retaining Austenite in I.C. Annealed Dual Phase Steels

Figure 34 gives an idea about the extent of manganese segregation that can take place in the austenite of a typical dual phase steel during intercritical annealing.

The M_s temperature of the steel with the composition mentioned in the figure, is given by the following empirical relation[132].

$$M_s = 539 - 423C - 20.4\ Mn - 17.7\ Ni - 12.1\ Cr - 7.5\ Mo = 468.02°C$$

For the sake of simplicity, consider that the concentration of manganese segregated after holding at 740°C for 60 minutes is 2 wt% although the nominal concentration is lower. Under such conditions the concentration of carbon needed to bring the M_s temperature down to room temperature (i.e. 20°C) would be

$$20 = 539 - 423C - 20.4 \times 3$$

or wt/% C = 1.08

This concentration of carbon is even beyond the level that can be achieved through complete partitioning ($\sim$ 0.7 wt%) into the austenite at 740°C, which is very unlikely to occur. Even if complete partitioning happens to take place after holding for 60 minutes, M_s temperature will be 181.7°C.

Austenite retained in dual phase steels has been observed to remain untransformed down to -269°C. The effect of austenite particle size therefore accounts for the suppression of M_s through an additional (181.7°C + 269°C) = 450.7°C. This clearly indicates that the suppression obtained due to the austenite particle size effect (450°C)

is more than that obtained due to the effect of chemical stabilization (which is 468.02-181.7 = 286.32°C).

It should be mentioned however, that dual phase steels are generally found to contain γ_R when subjected to short holdings[35,120] (1 to 5 minutes) at annealing temperatures. Although data for manganese and carbon concentration in γ_R under such conditions are not available, it is very likely the segregation of these two elements will not be significant. Thus, of the two stabilization mechanisms that contribute to the retention of austenite in these steels, the stabilization due to austenite particle size effect is more potent in suppressing the M_s.

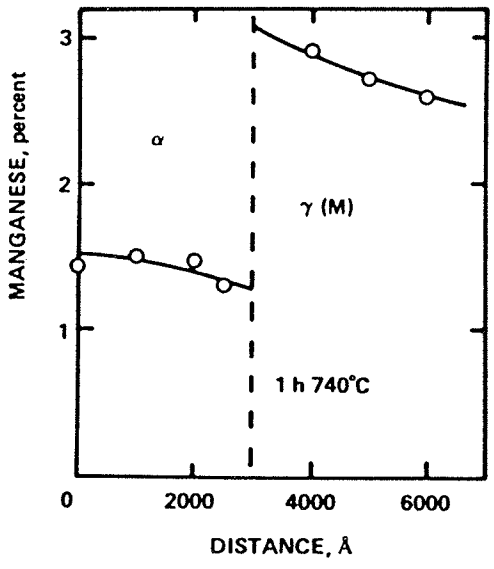

Figure 34. Manganese concentration of ferrite and austenite phases in 0.6C - 1.5 Mn steel after 1 h at 740°C as determined by scanning transmission electron microscope technique[133].

APPENDIX II

PRINCIPLES AND TECHNIQUES FOR RETAINED AUSTENITE MEASUREMENT BY X-RAY DIFFRACTION

Theoretical Considerations and Basic Equations

When a crystalline substance is irradicted by x-rays it produces a characteristic diffraction pattern which is determined by the crystal structure of all phases present with the substance[133].

Quantitative determination of the relative volume fractions of martensite and austenite can be made from x-ray diffraction charts because the x-ray intensity diffracted from each phase is proportional to the volume fraction of that phase. Furthermore if the phase contains a completely random arrangement of crystals and is of infinite thickness, so that x-rays do not pass through the sample the diffracted intensity from any single (hkl) plane within that phase is also proportional to the volume fraction of that phase. Thus on random specimens measurements of the integrated intensity of just one austenite and one martensite (hkl) line will accurately establish the volume fraction of each phase[130]. If however preferred orientation or texture is present within the specimen, intensity measurement may have to be made on at least four austenite and martensite lines, each to provide an accurate result by averaging. Since this study did not involve the use of specimens containing texture or preferred orientation of any relevant phase, this appendix will refer to randomly oriented grains unless specified.

The integrated intensity of a particular (hkl) reflection in the α or γ phase can be expressed as:

$$I_{\alpha}^{hkl} = \left(\frac{I_o e^4}{m^2 C^4}\right) \left(\frac{\lambda^3 A}{32\pi r}\right) \frac{1}{v^2} \left[|FF| p\ LP e^{-2M}\right] A(\theta)\ (V_{\alpha}) \qquad (a)$$

where I_{α}^{hkl} = integrated intensity per unit length of diffraction line (hkl) of the phase (α-phase in this case)

I_o = intensity of the incident beam

e, m = charge and mass of the electron

r = radius of the diffractometer

c = velocity of light

λ = wavelength of incident radiation

A = cross-sectional area of the incident beam

V = volume of the unit cell. $\frac{1}{v^2}$ defines the number of cells diffracting in the specimen

$|FF|$ = structure factor times its complex conjugate

p = multiplicity factor of the (hkl) reflection

L.P = Lorentz-polarization factor = $\frac{(1+\text{Cos}^2 2\theta)}{\text{Sin}^2\theta\text{Cos}\theta}$ for normal diffractometric analysis, but becomes $\frac{(1+\text{Cos}^2 2\alpha.\text{Cos}^2 2\theta)}{\text{Sin}^2\theta\text{Cos}\theta(1+\text{Cos}^2 2\alpha)}$ when a monochrometer is used, 2α is the diffraction angle of the monochrometer crystal

e^{-2M} = Debye-Waller or temperature factor

$A(\theta)$ = absorption factor. It is a function of θ and enters in as $\frac{1}{2\mu}$ where μ is the linear absorption co-efficient of the material for the specific x-ray radiation used

θ = angle of diffraction

V_{α} = volume fraction of the α-phase

Equation (a) can be simplified as follows:

$$I_\alpha^{hkl} = \frac{k.R_\alpha^{hkl}V^\alpha}{2\mu} \qquad (b)$$

where $$k = \left(\frac{I_o e^4}{m^2C^4}\right) \left(\frac{\lambda^3 A}{32\pi r}\right) \qquad (c)$$

and $$R_\alpha^{hkl} = \frac{1}{V^2}\left[|FF|\ p\ LPe^{-2M}\right] \qquad (d)$$

Thus k is a constant dependent only on selection of instrument geometry and radiation (i.e. wavelength) but completely independent of the nature of the specimen. R is a factor which depends on hkl, θ and the crystal structure and composition of the specimen or phase being measured. R can be calculated from basic principles, as will be stated later. The significance of R^{1kl} is that it is proportional to the integrated intensity which should be diffracted by a specific (hkl) reflection, when 100% of that phase exists and no preferred orientation is present. For the case of steel where two phases generally exist equation (b) is written more correctly as:

$$I_\alpha^{hkl} = \frac{R_\alpha^{hkl}\ V_\alpha}{2\mu_m} \qquad (e)$$

where μ_m is the linear absorption co-efficient for the mixture of martensite and austenite. A similar equation applies to the austenite or γ-phase. Thus the following can be written for any pair of hkℓ lines

$$\frac{I_\alpha^{hkl}}{I_\gamma^{hkl}} = \frac{R_\alpha^{hkl}\ V_\alpha}{R_\gamma^{hkl} V_\gamma} \qquad (f)$$

or $$\frac{V_\gamma}{V_\alpha} = \frac{I_\gamma^{hkl} R_\alpha^{hkl}}{I_\alpha^{hkl} R_\gamma^{hkl}} \qquad (g)$$

If martensite and austenite are the only phases present in a steel, they must make up 100% by volume. Therefore

$$V_{\gamma} + V_{\alpha} = 1 = 100\% \qquad (h)$$

Calculation of the Theoretical Relative Intensity Factors (R)

The solution of equation (h) depends on the calculation of R_{γ} and R_{α} factors for all the (hkl) lines used with the equations. The other variables, I_{γ}, and I_{γ} are quantities measured from the x-ray diffraction pattern.

As stated earlier, R-factors are functions of θ, hkl and the substance, and can be calculated from basic principles using equation (d). Each element of this equation may be determined as follows:

i) θ, is the Bragg angle of reflection for each martensite and austenite (hkℓ) line and depends on λ, the characteristic wavelength of the x-ray radiation selected. It is derived from the 2θ position of the peak maximum on sharp lines or from the centroid of area when the diffraction lines are broad. θ can also be calculated from lattice constants for austenite and martensite.

ii) Each θ-value is then used to calculate, the Lorentz-polarization (LP) factor, the temperature factor (e^{-2M}) and the atomic scattering factors $|f|$ which enter into the calculation of the structure factor $|FF|$ in equation (d) as follows

$$|FF| = [E(|f| - \Delta f)]^2$$

where $|f|$ is the atomic scattering factor for Fe, Mn and other alloying elements existing in the steel[134]. Δf is a correction for anomalous scattering[135] and E is the of atoms per unit cell which is 4 for FCC and 2 for BCC.

iii) The unit cell volume (v) is calculated for the lattice parameters of martensite and austenite which are themselves functions of the carbon and alloy content. Ordinarily the effects of alloy content on cell parameters in low and medium alloy steels and can be ignored but that of carbon cannot be done since cell dimensions do change significantly by the presence of carbon as shown by the following equation[134].

Phase	Crystal Structure	Change in Cell Parameters Due to Carbon
Martensite (untempered)	BCT	a = 2.867 - 0.013% C by weight
		c = 2.867 + 0.116% C by weight
Austenite	FCC	a = 3.555 + 0.044% C by weight

iv) The multiplicity factor (p) in equation (d) is dependent on the number of multiple reflections permitted by each (hkℓ) plane present within each phase (Reference[134], p.477).

It may be noted here that calculation of R-factors should be made for each type of steel if the composition is known. However if this cannot be done, general R factors calculated from common or average steel composition will provide acceptable accuracy if used for all steels[134].

A sample calculation of R for the (200) austenite line with Cu radiation is given in the following pages for the steel used in this study. It refers to a sample with a tempered martensite starting microstructure that was annealed at 762°C for 3 minutes and then cooled in air.

$$\text{Equation } R_\gamma(200) = \frac{1}{v^2} \left[|FF|p.LP \right] e^{-2M}$$

2θ = 50.731 for (200) γ line, obtained from the Philips PW-1710 Automated Powder Diffractometer in the Mineralogy laboratory of the Earth Science Department using a standard scanning programme.

Volume of unit cell, i.e. $v = a^3$ where $a = 3.555 + 0.044x = 46.1061$

$v^2 = 2125.7724$

Atomic Scattering factor f corresponding to

$$\text{Sin } \theta/\lambda = \frac{0.42839}{1.54178} = 0.278 \text{ (for Cu } k_\alpha \text{ radiation)},$$

for various constituents (chemical) in the steel was obtained from standard tables.

Table (a)

Showing details of calculations of the structure factor corresponding to (200) γ line

Element	wt %	f		Δf	=	f'	wt fract f'
Mn	1.63	16.32	+	0.66	=	15.66	0.2548
S	0.018	9.335	+	0.34	=	9.675	0.002
P	0.012	8.791	+	0.20	=	8.991	0.001
Si	0.11	8.646	+	0.15	=	8.614	0.009
Cu	0.34	18.714	+	(-2.62)	=	16.094	0.0547
Ni	0.07	17.97	+	(-3.75)	=	14.22	0.009
Cr	0.06	14.904	+	(-0.40)	=	14.504	0.008
V	0.062	14.182	+	0.00	=	14.182	0.009
Cb	0.024	27.878	+	(-1.38)	=	26.498	0.006
Mo	0.038	28.7	+	(-1.30)	=	27.4	0.01
Sn	0.10	35.054	+	(-1.25)	=	33.804	0.033
Fe	97.536	16.326	+	(-1.68)	=	14.646	14.285
				f' (weighted sum)			14.681

Δf values for different elements as functions of $\lambda/\lambda k$ and δ_k was also obtained from appropriate tables.[135]

Structure factor $F = 4\ (f + \Delta f) = 4f'$

Thus $|FF| = (4f')^2 = 16f'^2 = 16 \times (14.681)^2 = 3448.5082$

Multiplicity factor $p = 6$.

Temperature factor, $e^{-2M} = 0.94$, this value was taken from the curve in figure 35.

Lorentz-polarization factor $L.P = \dfrac{1 + \text{Cos}^2\ 50.731}{\text{Sin}^2(25.365) \times \text{Cos}(25.365)} = 8.46$

$$R_\gamma(200) = \frac{1}{v^2}\ [|FF|\ p.L.P.e^{-2M}]$$

$$= \frac{1}{2125.7721}\ [3448.5082 \times 6 \times 8.46 \times 0.94]$$

$$= 77.4041$$

Similarly for α (200), for which $2\theta = 65.023$.

Volume of unit cell, i.e. $v = a^2 \times c = 23.5196$

$v^2 = 557.825$

Atomic scattering factor f for iron and other alloying elements were obtained from standard tables corresponding to $\text{Sin}\theta/\lambda$

$$= \frac{0.53746}{1.54178} = 0.348$$

Table (b)

Showing the details of the calculation of the structure factor corresponding to α (200) α line

Element	wt %	f		Δf	=	f'	wt fract f'
Mn	1.63	14.794	+	(-0.63)	=	14.168	0.230
S	0.018	8.897	+	0.29	=	9.187	0.001
P	0.012	8.402	+	0.25	=	8.652	0.001
Si	0.11	8.1496	+	0.26	=	8.4096	0.009
Cu	0.34	17.770	+	(-2.62)	=	15.15	0.053
Ni	0.07	17.07	+	(-3.67)	=	13.4	0.009
Cr	0.06	14.09	+	(-0.40)	=	13.69	0.008
V	0.062	13.404	+	(-0.18)	=	13.224	0.008
Cb	0.024	26.608	+	(-1.35)	=	25.258	0.006
Mo	0.038	27.4032	+	(-1.36)	=	26.0432	0.01
Sn	0.10	33.555	+	(-1.25)	=	33.305	0.033
Fe	97.536	15.489	+	(-1.48)	=	14.009	13.66
				$4f'_\gamma$ (weighted sum)			14.028

As stated before Δf values were obtained from literature[b].

Thus $|FF| = 4f'^{\gamma} = 4 \times 14.028^2 = 787.139$

Multiplicity factor p = 4

Temperature factor, $e^{-2M} = 0.94$ (from Fig. 35)

$V^2 = 557.826$ using relevant values of a and c

$$L.P = \frac{1 + \text{Cos}^2\ 65.023}{\text{Sin}^2\ (32.511) \times \text{Cos}\ (32.511)} = 4.84$$

Therefore $R_\alpha(200) = \frac{1}{557.826}\ [787.139 \times 4 \times 4.84 \times 0.92]$

$= 25.133$

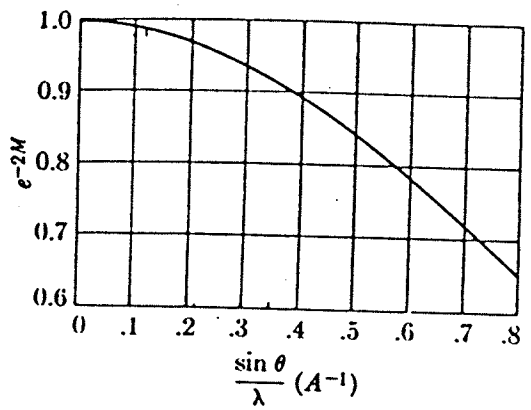

Figure 35. Temperature factor e^{-2M} of iron at 20°C as a function of $(\sin\theta)/\lambda$[134].

Measurement of X-ray Diffracted Intensities

In measuring the diffracted line intensities it is essential that integrated intensity be measured and not the maximum intensity. This is because large variations in line shape and broadening can occur in hardened and plastically deformed steels due to variations in microstructure and particle or grains size. These changes in line shape do not affect the integrated intensity but they can make the values of maximum intensity meaningless, even when apparently sharp lines are present.

Of the two techniques that are available for evaluating diffracted intensities from a specimen[129]: 1) measurement of areas above the background for each peak recorded on the chart paper and 2) electronic

integration of the area using a scaler circuit, the latter was used. It involved identifying the $\gamma(200)$ and $\alpha(200)$ peaks from trial scans. Each of these peaks were then scanned at a constant rate making sure that the 2θ range scanned was wide enough to include the whole peak. After subtracting the background over the 2θ range scanned for each peak, the ratio of the integrated intensities

$$\frac{I_{\gamma}^{(200)}}{I_{\alpha}^{(200)}}$$

was obtained. These values were obtained by running a programme using standard commands made available with the Philips PW-1710 Automated Powder Diffractometer.

For the sample considered in the sample calculation, the

$$\frac{I_{\gamma}^{(200)}}{I_{\alpha}^{(200)}} = 0.150$$

Using the values of I_{γ}

$$\frac{I_{\gamma}^{200}}{I_{\alpha}^{200}} \quad , \quad R_{\gamma}^{(200)} \quad , \quad R_{\alpha}^{(200)}$$

thus obtained from the above mentioned sample calculations in equation (f), the volume fraction of retained austenite is obtained through equation (h) which turns out to be 4.64%.